



OPEN ACCESS

EDITED BY

Stephen Nelson,
Brigham Young University, United States

REVIEWED BY

Peter Larson,
Washington State University,
United States
Gregory Roselle,
Brigham Young University-Idaho,
United States

*CORRESPONDENCE

Paolo Randazzo,
paolo.randazzo@unipa.it

SPECIALTY SECTION

This article was submitted to
Geochemistry,
a section of the journal
Frontiers in Earth Science

RECEIVED 17 May 2022

ACCEPTED 12 September 2022

PUBLISHED 30 September 2022

CITATION

Randazzo P, Caracausi A, Aiuppa A,
Cardellini C, Chiodini G, Apollaro C,
Paternoster M, Rosiello A and
Vespasiano G (2022), Active degassing
of crustal CO₂ in areas of tectonic
collision: A case study from the Pollino
and Calabria sectors (Southern Italy).
Front. Earth Sci. 10:946707.
doi: 10.3389/feart.2022.946707

COPYRIGHT

© 2022 Randazzo, Caracausi, Aiuppa,
Cardellini, Chiodini, Apollaro,
Paternoster, Rosiello and Vespasiano.
This is an open-access article
distributed under the terms of the
[Creative Commons Attribution License
\(CC BY\)](https://creativecommons.org/licenses/by/4.0/). The use, distribution or
reproduction in other forums is
permitted, provided the original
author(s) and the copyright owner(s) are
credited and that the original
publication in this journal is cited, in
accordance with accepted academic
practice. No use, distribution or
reproduction is permitted which does
not comply with these terms.

Active degassing of crustal CO₂ in areas of tectonic collision: A case study from the Pollino and Calabria sectors (Southern Italy)

Paolo Randazzo^{1*}, Antonio Caracausi², Alessandro Aiuppa¹, Carlo Cardellini^{3,4}, Giovanni Chiodini⁴, Carmine Apollaro⁵, Michele Paternoster^{2,6}, Angelo Rosiello³ and Giovanni Vespasiano⁵

¹Department of Earth and Marine Sciences (DiSTeM), Università di Palermo, Palermo, Italy, ²Section of Palermo, National Institute of Geophysics and Volcanology (INGV), Palermo, Italy, ³Department of Physics and Geology, Università degli Studi di Perugia, Perugia, Italy, ⁴Section of Bologna, National Institute of Geophysics and Volcanology (INGV), Bologna, Italy, ⁵Department of Biology, Ecology and Earth Sciences (DiBEST), University of Calabria (UniCAL), Arcavacata di Rende, Calabria, Italy, ⁶Department of Sciences, University of Basilicata, Potenza, Italy

Carbon dioxide (CO₂) is released from the Earth's interior into the atmosphere through both volcanic and non-volcanic sources in a variety of tectonic settings. A quantitative understanding of CO₂ outgassing fluxes in different geological settings is thus critical for decoding the link between the global carbon budget and different natural processes (e.g., volcanic eruption and earthquake nucleation) and the effects on the climate evolution over geological time. It has recently been proposed that CO₂ degassing from non-volcanic areas is a major component of the natural CO₂ emission budget, but available data are still sparse and incomplete. Here, we report the results of a geochemical survey aimed at quantifying CO₂ emissions through cold and thermal springs of the tectonically active Pollino Massif and Calabrian arc (Southern Italy). The chemical and isotopic (He and C) composition of fifty-five dissolved gas samples allows to identify two different domains: 1) a shallow system dominated by gas components of atmospheric signature (helium, hereafter He) and biogenic origin (C), and 2) a deeper system in which crustal/deep fluids (CO₂ and He) are dominant. The measured He isotope ratios range from 0.03 to 1.1 Ra (where Ra is the He isotopic ratio in the atmosphere) revealing a variable atmospheric contamination. Furthermore, the He isotopic data indicate the presence of traces of mantle He contributions (2%–3%) in the thermal groundwater. The prevailing low R/Ra values reflect the addition of crustal radiogenic ⁴He during groundwater circulation. Using helium and carbon isotope data, we explore the possible sources of fluids and the secondary processes (dissolution/precipitation) that act to modify the chemistry of pristine volatiles. For the thermal springs, we estimate a deep C output of 2.3 × 10⁷ to 6.1 × 10⁸ mol year⁻¹. These values correspond to deep CO₂ fluxes per square km comparable with those estimated in several active and inactive volcanic areas and in continental regions affected by metamorphic CO₂ degassing (e.g., the southern margin of the Tibetan Plateau).

KEYWORDS

helium, carbon dioxide, tectonic, Earth degassing, metamorphism

1 Introduction

The current rise in atmospheric CO₂, and its link with the global climate change, provides a strong motivation to understand the natural processes that control the nature and magnitude of geological CO₂ cycling (Evans, 2011). The release of carbon dioxide into the atmosphere *via* Earth degassing has played a crucial role in controlling global planetary temperature over geological time *via* the greenhouse effect (Foster et al., 2017). The modes and rates of geological CO₂ release are thus crucial to understand the compositional evolution of the atmosphere through geological time, life on Earth, and climate changes (Berner and Lasaga, 1989; Kerrick, 2001; Dasgupta, 2013; Aiuppa et al., 2019; Fischer and Aiuppa, 2020; Guo et al., 2021). Despite continuous improvements *via* direct measurements, models, and global extrapolations, the CO₂ Earth degassing output remains poorly constrained, hampering full understanding of the geological carbon cycle (Berner and Lasaga, 1989; Burton et al., 2013; Fischer, 2013; Fischer et al., 2019; Fischer and Aiuppa, 2020). The release of CO₂ from the Earth's interior into the atmosphere occurs in different tectonic settings (Lee et al., 2019), through volcanic and non-volcanic sources, and on a global scale, it is known that CO₂ discharges are associated with tectonically/seismically active zones (Barnes et al., 1978; Chiodini et al., 2004; Tamburello et al., 2018). Quantitative estimates of CO₂ outgassing fluxes in different tectonic settings are thus critical for decoding the link between the global carbon budget and climate evolution from a whole-Earth carbon cycling perspective (Zhang et al., 2021). In the last decades, the number of studies on CO₂ degassing in non-volcanic areas has risen exponentially, emphasizing the important contribution of these areas to the Earth carbon budget (e.g., Chiodini et al., 2020, 2004; Minissale, 2004; Becker et al., 2008; Italiano et al., 2008; Groppo et al., 2022, 2017, 2013; Rolfo et al., 2015; Lee et al., 2016; Tamburello et al., 2018; Caracausi and Sulli, 2019; Frondini et al., 2019). The first regional-scale CO₂ Earth degassing studies led to the catalogue of Italian CO₂-rich gas emissions (googas.ov.ingv.it and www.magadb.net) and to the regional map of deeply derived CO₂ degassing in central Italy that uses the quantification of carbon dissolved in regional groundwater systems (Chiodini et al., 2000; 2004; 2011). Some studies (Chiodini et al., 2004, 2020; Miller et al., 2004) also demonstrated a relation between CO₂ degassing and seismogenesis in the Italian Apennines, pointing to the presence of gas triggering earthquakes. The Mt. Pollino region, at the southern end of the Apennines (southern Italy), has been historically recognized as one of the most hazardous seismic gaps in the intra-Appennine seismogenic belt (Napolitano et al., 2021), but it has recently been affected by seismic sequence occurred between 2010 and 2014 and characterized by about

10,000 earthquakes with highly variable magnitude (strongest events ML 4.3 and ML 5.0; De Matteis et al., 2021; Pastori et al., 2021). Moreover, recent studies identified fluid-related dynamics responsible for historical and recent seismicity of the area (Sketsiou et al., 2021). The Calabrian arc, further to the south, is one of the most active seismogenic areas in Italy (Italiano et al., 2010; Neri et al., 2020), which has been repeatedly affected by catastrophic seismic events with $5.9 < M < 7.2$ during the last centuries (18 times from 1626 to 1908; Gruppo di Lavoro CPTI, 2004; Boschi et al., 2000). The two areas are characterized by the presence of several springs, some representing low-enthalpy geothermal resources (Zarlenga, 2011; Vespasiano et al., 2014, 2015a, 2015b, 2015c, 2016, 2021; Apollaro et al., 2015, 2016, 2020). The geochemical and isotopic compositions of Calabrian and Pollino waters have previously been investigated to define their geochemical features and geothermal potential (Bencini and Ciracò, 1982; Duchi et al., 1991), to investigate a link with seismicity and implications for a fluid–fault relationship (Gurrieri et al., 1984; Calcara and Quattrocchi, 1993; Italiano et al., 2010; Apollaro et al., 2020) and to evaluate potential natural metal contamination of spring waters (Margiotta et al., 2012, 2014; Paternoster et al., 2021). However, no attempt has been made so far to model the water–gas interaction processes and to quantify the regional-scale budget of CO₂ sequestered/transported by aquifers at depths and released into the atmosphere upon spring discharge.

In this study, we present the results of a geochemical study of cold and thermal springs from both the Calabrian arc and the Pollino region. Our goals are to 1) investigate the relationships between Earth degassing and geological features in the two areas; 2) assess the presence and eventual origin of deep volatiles released in the hydrothermal basins and the surrounding areas; 3) model the processes at depths that can modify the pristine chemistry of deeply rising volatiles, potentially affecting the deep carbon budget; and 4) estimate the total deeply derived CO₂ output. For this aim, we combine helium isotopes (³He/⁴He), total dissolved inorganic carbon (TDIC), and dissolved carbon isotopes (δ¹³C_{TDIC}) of groundwaters to explore the origin of carbon and to develop a model of water–gas–rock interaction. The results are then compared with the CO₂ output from some active tectonic regions and volcanic areas worldwide.

2 Geological and hydrogeochemical background

The Calabrian–Peloritani Orogen (CPO) is a well-developed, arc-shaped segment of the circum-Mediterranean orogenic belt between the southern Apennines and the Sicilian Maghrebides, bounded by two main tectonic lineaments: the Sangineto line to

the north and the Taormina line to the south (Cirrincione et al., 2015; Tortorici, 1982a, Tortorici 1982b; Figure 1). Incorporation of the Calabria terranes into the Apennine–Maghrebian chain is related to the processes responsible for the formation of the Tyrrhenian Basin since the late Miocene (Alterberger et al., 2011 and reference therein). In this context, the Calabrian arc represents an accretionary wedge, caused by the collision of the Eurasian and African plates (Amodio Morelli et al., 1976; Tortorici, 1981), consisting of a series of ophiolite-bearing tectonic units (Liguride Complex; Ogniben, 1969) and overlying basement nappes (Calabride Complex; Ogniben, 1969) with Paleozoic metamorphic and plutonic terranes that represent the remnants of Caledonian, Hercynian, and Alpine orogens (e.g., Amodio Morelli et al., 1976; Schenk, 1981; Zanettin Lorenzoni, 1982; Atzori et al., 1984; Del Moro et al., 1986; Zeck, 1990; Messina et al., 1994). The CPO is classically subdivided into a northern and southern sector, separated in correspondence to the Catanzaro Strait Basin, a Neogene–Quaternary basin connecting the Ionian and Tyrrhenian seas (Tortorici, 1982a; Chiarella et al., 2012, 2016; Longhitano et al., 2014; Brutto et al., 2016). The two sectors differ for the structural style and assemblage of the chain. The northern block exhibits overthrust of alpine and pre-alpine crystalline units on carbonate tectono-stratigraphic units. In the southern block, the chain is made up of alpine and pre-alpine crystalline units, while the Apennine carbonate rocks are not present beneath the crystalline–metamorphic units (Apollaro et al., 2019a and reference therein). In particular, the Calabria arc terrane consists of three main groups of stacked tectonic units (Tursi et al., 2021) that can be summarized, from bottom to top, as follows: 1) the Lower Complex, characterized by Apennine units with Meso-Cenozoic phyllites and partly metamorphosed carbonate rocks exhibiting high pressure (1.4 GPa) and low temperature (390°C) metamorphic imprint (Iannace et al., 2007); 2) the Intermediate Complex, composed of ophiolite units of the Ligurian Tethys’ oceanic lithosphere (Liberi et al., 2006), which records *HP/LT* Eocene metamorphism with peak conditions at 2.0–2.1 GPa and 470–490°C (Tursi et al., 2020); and 3) the Upper Complex, which consists of the Hercynian continental crust, showing a local Alpine metamorphic overprint at 0.3–0.7 GPa and 200–450°C in the Sila Massif and Catena Costiera (Piccarreta, 1981; Acquafredda et al., 1994; Graessner and Schenk, 2001; Liberi et al., 2011; Ortolano et al., 2020) and up to 1.1–1.2 GPa and 540–570°C in the Aspromonte Massif (Cirrincione et al., 2008). According to the current geodynamic models, the evolution of the Calabrian arc was driven by the south-eastward retreat of the Ionian slab (Malinverno and Ryan, 1986; Jolivet and Faccenna, 2000; Faccenna et al., 2001). During the Eocene, subduction of the Ligurian Tethys oceanic crust underneath the continental margin, represented by the Calabria terrane, (Stampfli and Borel, 2002; Rossetti et al., 2004; Vitale et al., 2019), is thought to have occurred at 47–20 Ma (Borsi and Dubois,

1968; Schenk, 1980; Beccaluva et al., 1981; Thomson, 1994, 1998; Rossetti et al., 2001, 2004; Shimabukuro et al., 2012). Currently, the active subduction residue of the ancient, 200-km wide, subducting slab dipping 70° towards NE is found beneath the Calabrian arc with the presence of deep seismicity (150–300 km) (Lucente et al., 1999; Spakman and Wortel, 2004; Chiarabba et al., 2008; Neri et al., 2009; Neri et al., 2012). Different studies show a rapid deepening of the Ionian Moho beneath Calabria, illustrating the geometry of the subduction zone (Piana Agostinetti et al., 2009; Scarfi et al., 2018). The estimated current plate convergence velocity between the two plates is 3–5 mm/year (Neri et al., 2020; Mattei et al., 2007), and the rollback of the subducting slab occurs at about 2 mm/year rate (Hollenstein et al., 2003; Devoti et al., 2008; Nocquet, 2012).

The Calabrian arc is one of the strongest seismic areas in Italy (Neri et al., 2020) has experienced several destructive earthquakes with estimated magnitudes of about 7 or higher (Scarfi et al., 2018). After the destructive 1908 earthquake (Rovida et al., 2016), a few events with $M > 4$ and about 200 shocks with a magnitude between 3 and 4 (out of a total of 3,800 events) have occurred between 1980 and 2005 (Gruppo di Lavoro CPTI, 2004; Castello et al., 2006). Crustal thickness reaches about 35–38 km in correspondence of the highest portion of the chain (Di Stefano et al., 2009), and the recorded seismicity is marked by focal depths <30 km (i.e., crustal depths; Neri et al., 2020; Boschi et al., 2000). Since the Middle Pleistocene, an intense WNW–ESE-oriented regional extensional phase occurred, resulting in a longitudinal faults system with NNE–SSW strikes and parallel to the mountain system (Figure 1A), consisting of a 10–50 km-long distinct normal fault segment running along the western side of the Calabrian arc (Tansi et al., 2005; Catalano et al., 2008). The development of the rift-zone, coupled with contrasting vertical movements, such as mountain chain uplifting of 0.5–1.2 mm/year in the last 1–0.7 Myr (Monaco et al., 1996; Ferranti et al., 2008; Faccenna et al., 2011), is still an active process (Dumas and Raffy, 2004) and probably represents the response to the isostatic rebound due to the detachment of the Ionian-subducted slab (Tortorici et al., 2003; Tortorici et al., 1995 Westaway, 1993). GPS data show differential motion of the Calabrian arc relative to both the Nubia and Eurasia plates, which causes active extension on the region with the developments of the aforementioned extensive faults (Mattei et al., 2007 and reference therein). These normal faults are considered to be major seismogenic faults (Monaco et al., 1996; Neri et al., 2006), with the NE trending fault systems of the Messina Straits, Gioia Basin, and Mesima Valley believed to have generated the major earthquakes of the area (Rovida et al., 2019, 2020; Neri et al., 2020).

The first comprehensive geochemical data-set for fluids circulating over the Calabrian arc has been presented by Italiano et al. (2010). The authors used the chemical and isotopic (C and He) compositions of groundwater and dissolved gas to show the aquifers contain deeply derived

CO₂-rich gas with a radiogenic He signature, a consequence of long residence in the crust. Clear fault–fluid relationships have been found in some of the investigated sites, with the thermal character of the investigated waters being linked with deeper hydrological circuits and normal geothermal gradients (30°C/km). Recent studies have reconstructed the conceptual geothermal model of some Calabrian sites using a “site-specific” (Vespasiano et al., 2021), multidisciplinary approach, involving geological, hydrogeological, and geochemical data. These studies highlighted different features between the thermal waters from north to south, related to complex geologic and tectonic settings of the region (e.g., Apollaro et al., 2012, 2016, 2019a, 2019b, 2019c, 2020, 2021; Vespasiano et al., 2012, 2014, 2015a, b, 2015c, 2016). Moreover, a deep component for dissolved gases of Pollino water have been identified from Apollaro et al. (2020) on the base of their C and He isotopic compositions.

3 Sampling and analytical methods

In total, 55 water samples were collected (see Figure 1) during two field campaigns in February and July 2019 (Table 1). Water temperature, pH, Eh, and electrical conductivity (EC) were measured *in situ* by means of high-resolution multi-parametric probes (Hanna Instruments HI-9828). Total alkalinity was measured *in situ* by acidimetric titration with 0.05 N HCl using methyl-orange as the indicator. The water samples were filtered *in situ* through a 0.45- μ m pore-size membrane and acidified with supra-pure HNO₃. Different sample aliquots (one filtered and two filtered and acidified) were collected. All samples were stored in high-density polyethylene bottles for laboratory analysis. Major elements were determined by high-performance liquid chromatography (HPLC) by using a Thermo Scientific Dionex™ ICS-1100 equipped with Dionex IonPac AS23 and Dionex IonPac CS12A columns for the determination of anionic (F⁻, Cl⁻, SO₄²⁻, and NO₃⁻) and cationic (K⁺, Na⁺, Ca²⁺, and Mg²⁺) species, respectively. The computed charge balance resulted <5% in all water analyses. All measurements were performed at the Department of Biology, Ecology and Earth Sciences laboratories of the University of Calabria (Cosenza, Italy). TDIC and saturation indexes (SI) with respect to the mineral phases (calcite, dolomite, and gypsum) were calculated using the PHREEQC Interactive computer code (Parkhurst and Appelo, 1999), considering the measured pH, the temperature, and the water composition.

The water samples used for the analysis of dissolved gases, $\delta^{13}\text{C}$ of TDIC, He and Ne isotopes (³He, ⁴He, and ²⁰Ne) were sampled in glass bottles according to Capasso and Inguaggiato (1998) and analyzed in a few days from their collection to prevent any contamination and/or loss of volatiles. The chemical composition of the dissolved gases was analyzed

by using the method described by Capasso and Inguaggiato (1998), which is based on the equilibrium partition of gas species between a liquid and a gas phase. The analysis was performed utilizing a Perkin Elmer Clarus 500 gas chromatograph equipped with a 3 m packed column (100/120 Shincarbon, Ar gas carrier) and two detectors, a thermal conductivity detector (TCD), and a flame ionization detector (FID), and using Ar as the carrier gas. H₂, O₂, N₂, and CO₂ were measured by means of the TCD, while CH₄ and CO were determined through a FID coupled with a methanizer. Analytical errors for CO₂, N₂, H₂, CO, CH₄, and O₂ are within 3%. Analyses of the dissolved noble gases (He and Ne) and He isotopic composition (³He/⁴He) were performed by using the methodology proposed by Inguaggiato and Rizzo (2004), which is based on the isotope equilibrium between the liquid and host gas phases (e.g., N₂). The extracted gases from waters are purified in a high-vacuum purification line that is directly connected to the mass spectrometers (Rizzo et al., 2019 and references therein). He and Ne isotopes are analyzed using a static vacuum mass spectrometer (GVI Helix SFT) with a double collector to detect ³He and ⁴He ion beams simultaneously with a multi-collector Thermo-Helix MC Plus mass spectrometer (isotopic ratio precision within $\pm 0.5\%$). The ³He/⁴He ratio was determined by measuring ³He in an electron multiplier detector and ⁴He in an axial Faraday detector. The isotopic composition of TDIC ($\delta^{13}\text{C}_{\text{TDIC}}$) is measured by using the method proposed by Capasso et al. (2005), using a Thermo Scientific Delta V Advantage continuous flow isotope ratio mass spectrometer. All $\delta^{13}\text{C}_{\text{TDIC}}$ values were reported relative to the Vienna Pee Dee Belemnite (VPDB) international reference standard, and the analytical precision is $\pm 0.15\%$. All sampling and analytical devices are provided by the Istituto Nazionale di Geofisica e Vulcanologia, Sezione di Palermo.

4 Results

The physico-chemical parameters of the collected waters are reported in Table 1 together with the computed TDIC values, chemical and isotopic compositions (He and C) of dissolved gases. Major ions water chemistry is presented in Supplementary Table S1. The 55 samples have been subdivided in two categories on the basis of their discharge temperature following the classification of Apollaro et al. (2020) and Italiano et al. (2010): cold (T < 20°C) and thermal (T \geq 20°C). The cold waters show compositions typical of shallow air-saturated waters (ASW) with N₂ concentrations ranging between 10.3 and 17.6 ccSTP/l and CO₂ from 1.5 to 24.4 ccSTP/l. O₂ concentrations are between 2.6 and 8.6 ccSTP, while CH₄, CO, and H₂ concentrations are very low (CH₄ \leq 5.5 \times 10⁻⁰⁴ ccSTP/l; CO \leq 3.5 \times 10⁻⁴ ccSTP/l; and H₂ \leq 1.6 \times 10⁻³ ccSTP/l). Both He and Ne are present in trace

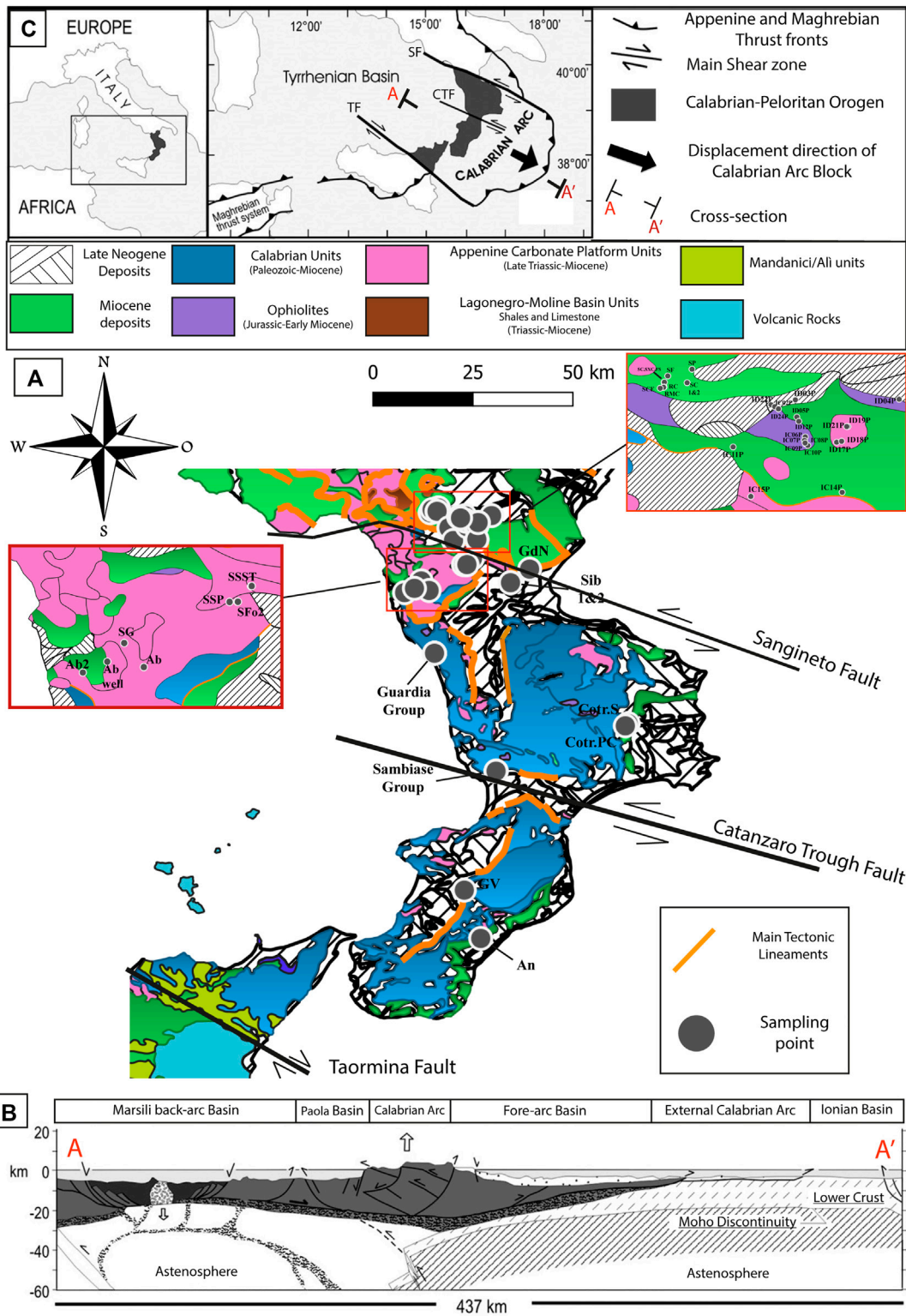


FIGURE 1

(A) Simplified geological map of the Calabrian arc and the surrounding region (modified after Amodio-Morelli et al., 1976 and Bonardi et al., 1988b) with (B) the geological section on the bottom (after Van Dijk and Scheepers, 1995; and Van Dijk et al., 2000; modified) and on top (C), the location of the study area and tectonic simplified sketch of the Calabrian arc (after Tansi et al., 2005, modified). TF, Taormina Fault; CTF, Catanzaro Trough Fault; SF, Sangineto Fault. For a detailed overview of the individual springs, see Paternoster et al. (2021), Apollaro et al. (2020), Apollaro et al. (2019c), Apollaro et al. (2012), Vespasiano et al. (2021).

TABLE 1 Location, physico-chemical parameters, flow rates, chemical and isotopic compositions of Calabria and Pollino springs. T—thermal; C—cold; < d.—below detection limits; - not measured.

Name	ID	Type	Coordinates		pH	T °C	Cond uS/ cm	Eh mV	Q l/s	TDIC mmol/ l	$\delta^{13}\text{C}_{\text{TDIC}}$ ‰ vs. PDB	He ccSTP/ l	O ₂ ccSTP/ l	N ₂ ccSTP/ l	CH ₄ ccSTP/ l	CO ₂ ccSTP/ l	Ne ccSTP/ l	⁴ He/ ²⁰ Ne	R/ R _a
			X	Y															
Fontana Solfurea	FS	T	583623.0	4438112.0	7.5	21.8	698	-207	0.41	4.4	-4.7	2.17E-03	0.17	13.12	2.9E-02	10.68	2.15E-04	10.1	0.10
Solfurea Cupola	SC	T	583619.0	4438165.0	7.5	21.8	710	-101	11	4.1	-4.8	1.38E-03	1.02	12.61	6.2E-03	11.12	2.29E-04	6.0	0.14
Sinistra Cupola	SXC	T	583644.0	4438165.0	7.4	21.5	689	-14	10	4.1	-5.1	1.25E-03	1.38	12.35	5.2E-03	10.94	2.06E-04	6.1	0.13
Ruscello Caldo	RC	T	583623.1	4437576.5	8.3	20.3	713	76	78	3.6	-4.2	<d.l	5.37	10.76	1.0E-04	1.27	-	-	-
Ruscello meno caldo	RMC	C	583576.1	4437538.5	8.2	19.0	699	97	135	3.4	-3.84	<d.l	5.94	10.30	9.6E-05	1.82	-	-	-
Sorgente Pargo	SP	C	586220.2	4439782.9	7.4	11.8	627	265	0.60	7.0	-15.5	5.66E-05	6.59	11.46	3.5E-05	2.75	1.98E-04	0.3	0.90
Sorgente Celano	SCE	T	583263.5	4437427.6	7.6	18.4	735	228	20	4.1	-4.02	<d.l	6.09	11.40	0.0E+00	19.82	-	-	-
Sorgente Fraccia	SF	C	583951.0	4438936.6	8.0	12.0	396	162	0.10	3.4	-13.2	7.06E-05	7.55	14.05	9.4E-05	1.60	2.25E-04	0.3	0.92
S. Latronico Centro 1	SC1	C	585776.6	4438117.9	8.1	10.1	368	220	0.10	3.5	-12.1	<d.l	6.41	11.87	5.5E-04	3.58	-	-	-
S. Latronico Centro 2	SC2	C	585776.6	4438117.9	7.9	10.7	460	240	0.07	3.9	-14.1	<d.l	5.04	11.27	5.5E-05	4.80	-	-	-
Sorgente Serra	SS	C	598892.8	4415866.0	8.4	8.3	377	192	50	3.8	-9.1	<d.l	8.39	12.86	7.9E-05	2.45	-	-	-
Sorgente tufarazzo	ST	C	599003.9	4415898.8	8.3	6.7	366	202	90	3.7	-11.3	<d.l	8.64	13.09	9.0E-05	1.50	-	-	-
Sorgente san paolo	SSP	C	595778.0	4412859.0	7.9	10.4	347	245	15	3.6	-11.0	<d.l	7.61	13.04	4.2E-05	4.46	-	-	-
Sogente foce	SFo	C	596945.0	4412912.0	7.6	10.5	350	265	101	3.6	-11.3	6.81E-05	6.87	12.90	0.0E+00	5.53	2.49E-04	0.3	1.09
Sogente foce 2	SFo2	C	597003.0	4412912.0	7.7	11.1	352	260	101	3.6	-9.4	<d.l	6.73	13.47	5.8E-05	5.25	-	-	-
Sorgente Guaglianone	SG	C	580341.4	4404915.4	7.6	11.2	456	258	20	4.7	-9.3	<d.l	6.37	10.96	0.0E+00	8.22	-	-	-
Abatemarco 2	Ab2	C	574291.6	4399292.9	7.4	12.1	804	258	50	4.2	-11.3	<d.l	4.70	13.00	0.0E+00	8.68	-	-	-
Solfurea abatemarco	AbS	C	582183.9	4399373.5	7.3	12.5	880	64	1.50	6.0	-12.2	9.45E-05	2.65	14.02	1.2E-04	24.42	2.69E-04	0.4	0.75
Sorgente Abatemarco	Ab	C	583278.7	4400412.0	7.9	8.5	295	227	634	2.8	-13.4	<d.l	7.93	13.29	5.2E-05	2.73	-	-	-
Pozzo abatemarco	Ab well	C	577884.1	4401371.0	7.4	13.2	512	277	10	5.6	-12.4	7.53E-05	6.00	17.62	0.0E+00	21.57	2.86E-04	0.3	0.99
Grotta delle ninfe	GdN	T	620010.3	4411051.4	7.4	26.2	1103	-255	70	4.4	-8.6	1.15E-03	0.04	11.31	1.9E-01	13.30	1.95E-04	5.9	0.05
Sibarite 1	Sib1	T	613100.1	4404494.9	7.3	24.2	1086	-253	0.70	4.8	-8.3	1.79E-03	0.05	11.55	3.5E-02	11.47	1.90E-04	9.4	0.17
Sibarite 2	Sib2	T	613100.1	4404494.9	7.4	23.7	1088	-266	10	4.6	-8.3	2.23E-03	0.08	14.26	4.2E-02	12.22	2.33E-04	9.6	0.17
Tarantola Nuova	IC02P	C	594115.7	4435291.2	6.7	11.2	488	429	22.5	7.0	-14.9	-	-	-	-	-	-	-	-
Fosso S. Arcangelo	ICP06P	C	596944.0	4431641.7	7.1	11.1	701	552	0.45	9.1	-20.6	1.80E-04	5.23	13.22	4.40E-05	5.61	-	-	-
Fontana Pagnotella	ICP07P	C	596873.8	4431199.8	6.8	12.4	548	591	0.39	6.5	-19.3	<d.l	3.79	11.26	7.79E-05	4.69	-	-	-
Fontana di Mezzo	IC09P	C	596983.4	4430781.8	6.9	12.3	434	516	0.25	5.2	-18.8	-	-	-	-	-	-	-	-
Fontana Giudea	IC10P	C	597201.6	4430587.3	6.9	11.8	479	550	0.27	5.8	-20.0	1.15E-04	3.30	13.12	4.18E-05	4.78	-	-	-
Sorgente Montagna Pastoroso	IC11P	C	590186.8	4430325.1	6.7	9.9	289	356	0.23	4.2	-15.4	<d.l	5.72	14.70	3.86E-05	2.77	-	-	-

(Continued on following page)

TABLE 1 (Continued) Location, physico-chemical parameters, flow rates, chemical and isotopic compositions of Calabria and Pollino springs. T—thermal; C—cold; < d.—below detection limits; - not measured.

Name	ID	Type	Coordinates		pH	T °C	Cond uS/cm	Eh mV	Q l/s	TDIC mmol/l	$\delta^{13}\text{C}_{\text{TDIC}}$ ‰ vs. PDB	He ccSTP/l	O ₂ ccSTP/l	N ₂ ccSTP/l	CH ₄ ccSTP/l	CO ₂ ccSTP/l	Ne ccSTP/l	$^4\text{He}/^{20}\text{Ne}$	R/ R _a
			X	Y															
Frida	IC14P	C	600498.7	4424909.8	6.8	6.0	320	457	525	2.4	-10.2	<d.l	5.38	14.84	3.05E-04	2.67	-	-	-
Mercure	IC15P	C	591921.7	4424289.0	6.8	10.7	357	571	2050	5.0	-10.9	-	-	-	-	-	-	-	-
Tarantola Nuova 2	ID02P	C	594115.7	4435291.2	7.0	11.5	494	353	5.5	3.6	-14.1	<d.l	5.92	12	5.34E-05	7.91	-	-	-
Acqua Ficavozza	ID03P	C	595955.3	4436159.1	6.8	13.2	278	337	2.7	3.2	-	-	-	-	-	-	-	-	-
Sorgente Altosano	ID04P	C	605692.6	4436356.2	6.9	12.3	683	321	0.06	4.7	-15.7	-	-	-	-	-	-	-	-
Sorgente Bosco Magnano	ID05P	C	596121.7	4434058.1	7.0	12.3	509	330	0.14	4.7	-17.5	-	-	-	-	-	-	-	-
Fontana Matarazzo	ID08P	C	596936.9	4430898.4	7.0	12.5	441	328	0.36	3.5	-16.5	-	-	-	-	-	-	-	-
Sorgente Timpa della Gatta (Cropani)	ID12P	C	596315.5	4433533.3	6.9	10.3	416	300	0.24	5.3	-19.3	-	-	-	-	-	-	-	-
Fontana Camauli - Sorgente Costa Cirasa	ID17P	C	599896.5	4431020.0	7.0	9.3	298	603	2	3.2	-13.9	-	-	-	-	-	-	-	-
Fontana Mancini - Sorgente Mancini	ID18P	C	600366.6	4431152.6	6.8	8.8	315	355	1.5	4.2	-13.3	-	-	-	-	-	-	-	-
Sorgente Murge Muretto	ID19P	C	600942.4	4432958.0	7.1	9.7	397	340	2	2.4	-15.0	-	-	-	-	-	-	-	-
Frida Alta	ID20P	C	600498.7	4424909.8	6.8	5.9	322	344	100	3.8	-9.1	-	-	-	-	-	-	-	-
Fontana Fosso del Pantano	ID21P	C	600816.9	4432950.2	6.7	11.3	270	229	0.03	6.6	-16.0	-	-	-	-	-	-	-	-
Miretta	ID22P	C	593688.7	4435523.3	7.0	11.2	483	341	2.2	3.4	-13.2	-	-	-	-	-	-	-	-
Tarantola Vecchia	ID23P	C	594030.3	4435302.4	7.0	11.2	493	348	0.50	3.7	-12.8	-	-	-	-	-	-	-	-
Curcio	ID24P	C	594386.7	4435026.2	7.1	11.8	496	338	1.2	3.6	-16.1	-	-	-	-	-	-	-	-
Galatro Vecchia	GV	T	597973.8	4257944.8	6.4	35.6	5370	-96	3	12.5	-9.2	1.02E-02	0.18	16.74	2.2E-01	0.19	3.21E-04	31.8	0.12
Antonimina	An	T	604399.2	4235058.8	7.0	20.0	1226	-41	0.5	3.7	-8.6	1.09E-01	0.11	14.20	1.7E-03	0.51	1.66E-04	658.7	0.03
Guardia Caronte	Gpcar	T	585607.7	4370563.8	6.3	35.9	5157	-67	5	11.2	-4.4	2.67E-03	0.04	0.00	2.5E+00	36.43	1.41E-04	18.9	0.11
Guardia Calda	GPC	T	585597.1	4370566.2	6.7	37.2	2,405	26	5	4.8	-4.7	2.55E-03	0.04	8.11	2.4E+00	33.08	1.67E-04	15.2	0.11
Guardia Fredda	GPF	T	585589.1	4370565.2	6.9	37.4	2,413	37	100	4.4	-5.8	6.24E-04	0.07	11.76	4.6E-01	11.96	1.97E-04	3.2	0.13
Sambiase 1	Sam1	T	609125.3	4314733.7	6.6	36.8	2,292	42	60	6.0	-5.1	2.59E-03	0.03	9.95	1.2E-01	14.27	1.93E-04	13.4	0.14
Sambiase 2	Sam2	T	609074.3	4314786.3	6.8	35.9	2,520	87		4.9	-6.7	1.12E-03	0.12	12.65	8.1E-02	10.46	1.63E-04	6.9	0.13
Sambiase fiume	SamF	T	609053.0	4314732.1	6.6	20.3	1690	49		5.9	-4.5	2.69E-03	0.05	11.14	1.2E-01	12.88	1.86E-04	14.5	0.15
Sulfurea Cotronei	Cotr.S	T	657615.3	4338191.2	8.0	36.6	1995	118	0.6	0.8	-9.9	7.69E-05	0.08	13.09	2.0E-01	36.57	1.89E-04	0.4	0.51
Cotronei P. Coniglio	Cotr.PC	T	656593.0	4337113.0	7.7	35.2	15350	-7	1	1.1	-6.4	5.02E-02	0.11	22.60	4.5E-01	0.10	4.35E-04	115.3	0.08

amounts (up to 9.4×10^{-5} ccSTP/l and 2.9×10^{-4} ccSTP/l). In thermal waters, the measured He amounts are much higher (up to 0.11 ccSTP/l) than in cold samples, while Ne ranges between 1.4×10^{-4} and 4.3×10^{-4} ccSTP/l (Table 1).

In the ternary diagram $\text{CO}_2\text{-N}_2\text{-O}_2$ of Figure 2, thermal samples cluster along the $\text{CO}_2\text{-N}_2$ axis, as implied by their low to negligible O_2 contents (≤ 1.4 ccSTP/l). These samples have CO_2 concentrations from 0.1 to 36.6 ccSTP/l and N_2 concentrations from 0.004 to 22.6 ccSTP/l. Sample RC is the unique thermal sample falling close to the ASW field (Figure 2). This is because the sample was taken from a small stream exposed to the atmosphere and thus differs from other thermal samples from underground circuits not exposed to the atmosphere.

The $\delta^{13}\text{C}_{\text{TDIC}}$ ranges from -14.8‰ to -5‰ (vs. V-PDB) in cold samples and from -9.9‰ to -4.4‰ in thermal samples (Table 1).

The $^3\text{He}/^4\text{He}$ isotopic ratio (R) of each sample is normalized to the same ratio in air ($R_a = 1.386 \cdot 10^{-6}$; Ozima and Podosek, 2002). The R/R_a ratios range from 0.8 to 1.1 and from 0.03 to 0.5 R_a , for cold and thermal waters, respectively. The $^4\text{He}/^{20}\text{Ne}$ ratios are up to 659 for thermal samples, well above the ASW

ratio (0.295 at 25°C; Ozima and Podosek, 2002), indicating a negligible atmospheric contamination. On the contrary, the $^4\text{He}/^{20}\text{Ne}$ ratios of the cold waters, ranging between 0.26 and 0.35, indicate a dominant atmospheric derivation (Figure 3).

5 Discussion

In the following sections, we discuss the sources of fluids (both CO_2 and He) in the studied areas, and the secondary processes that affect the groundwater He- CO_2 signature during circulation and storage in the aquifers.

5.1 Helium

In natural fluids, He is typically fed by three distinct sources: the mantle, the crust, and the atmosphere (Sano et al., 1997). Each of these sources has a distinct He isotopic signature and $^4\text{He}/^{20}\text{Ne}$ ratio ($>1,000$ for crust and mantle, 0.295 for air-saturated water at 25°C; Sano and Marty, 1985; Ozima and Podosek, 2002). Therefore, the contributions of these three different sources can be solved by using binary mixing equations. Applying the approach of Sano et al. (1997), and assuming that all ^{20}Ne is of atmospheric origin, we estimated low

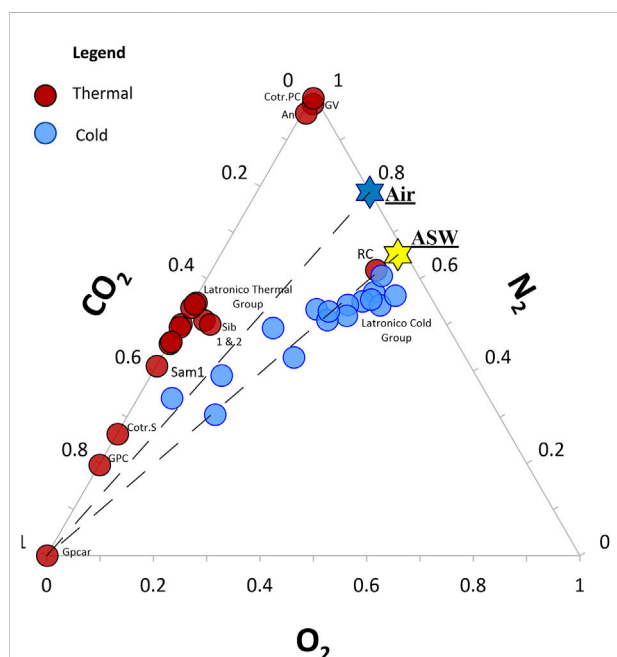


FIGURE 2
 $\text{CO}_2\text{-O}_2\text{-N}_2$ ternary diagram for the dissolved gas from cold and thermal springs. Thermal samples (red) fall along the axis between CO_2 and N_2 , as implied by their being the two dominant gas species, showing low O_2 values. The cold waters (blue circles) show compositions typical of shallow water falling on mixing line between the air-saturated water (ASW) and CO_2 -rich end member. The label Latronico Group refers to a group of samples from the Basilicata–Calabria border (Lucane thermal area). The cold group includes samples RMC, SP, SF, SC1, and SC2. The thermal group includes samples FS, SC, SXC, RC, and SCE. More information about these samples can be found in Apollaro et al. (2020).

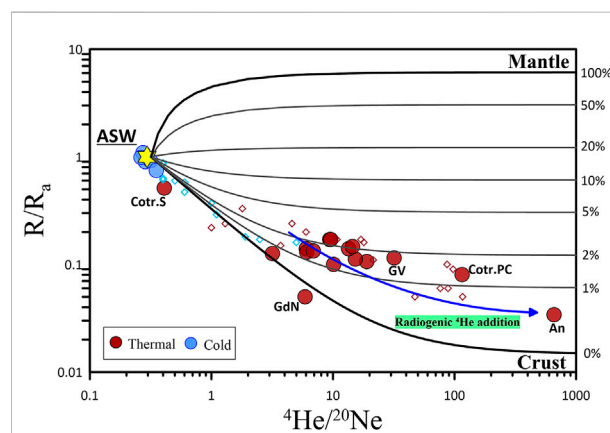
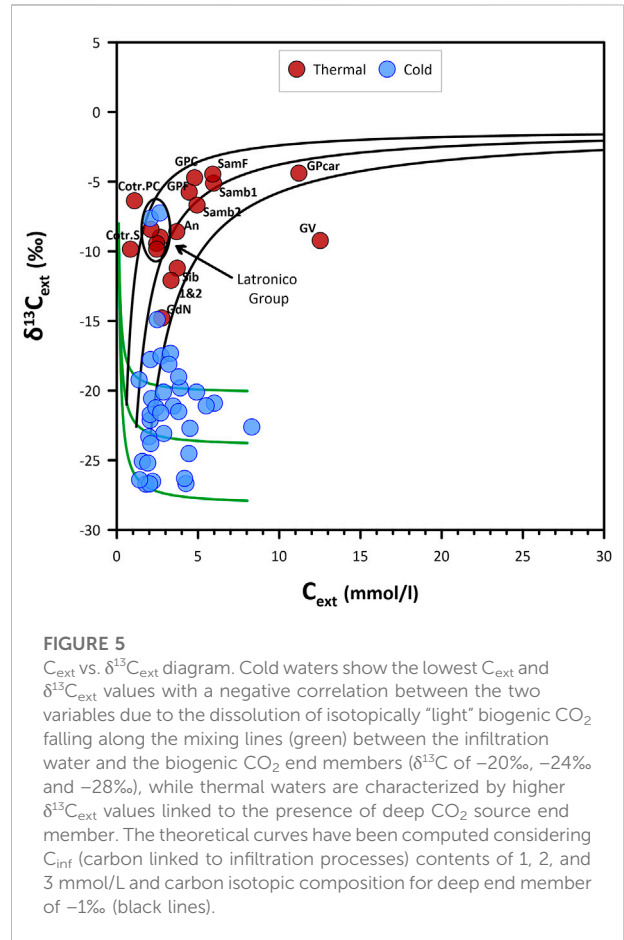
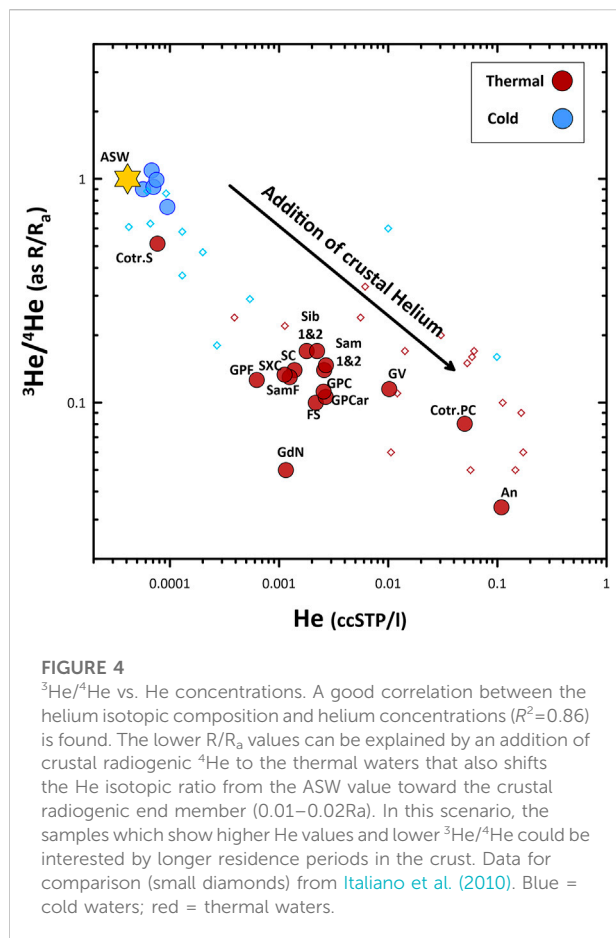


FIGURE 3
 $^3\text{He}/^4\text{He}$ ratios (expressed as R/R_a) versus $^4\text{He}/^{20}\text{Ne}$ ratios. All samples fall along mixing lines between three possible end-members characterized by distinct He isotopic signatures: 1 R_a , for air-saturated water (ASW; Ozima and Podosek, 2002); $0.01\text{--}0.02 R_a$, for pure crustal fluids dominated by radiogenic ^4He produced by U and Th decay (Ballentine and Burnard, 2002); and $6.1 \pm 0.9 R_a$, for the European subcontinental lithospheric mantle, ESCLM (Gautheron & Moreira, 2002) and $^4\text{He}/^{20}\text{Ne}$ values ($^4\text{He}/^{20}\text{Ne}$ ratios $>1,000$ for crust and mantle and 0.295 for ASW, respectively; Sano et al., 1985; Ozima and Posek, 2002). Thermal samples show helium isotopic composition near the crustal value of $0.02 R_a$ with small percentages in mantle contribution (2%–3%) and negligible atmospheric contamination, while cold waters and only one thermal sample show ASW-like composition. Data for comparison (small diamonds) from Italiano et al. (2010).

atmospheric contributions (<10%) for the thermal samples, along with small percentages (up to 2%–3%) of mantle He contribution, in agreement with the data reported by Italiano et al. (2010) (Figure 3). Dissolved gases from the cold waters and one thermal sample (Cotr.S) have an ASW-like composition, which indicates high atmospheric contamination probably due to a shallow hydrological circuit. We find a statistically significant ($R^2=0.86$) negative correlation between the He isotopic composition and its concentration (Figure 4). The lower R/Ra values of the He-rich thermal waters with respect to that of the cold waters is thus explained by the addition of crustal He, rich in radiogenic ^4He produced by U and Th decay (Ballentine and Burnard, 2002), during deep/prolonged circulation in the crust. It is noteworthy that the He-enriched samples have been collected in areas geologically dominated by metamorphic rocks characterized by high U and Th concentrations (e.g., 3.3 ppm of U and 19.4 ppm of Th for the “Sila” gneiss; Micheletti et al., 2007 and 297 ppm of U and 155 ppm of Th for zircons from the “Catena costiera” gabbros; Liberi et al., 2011). Hence, it is reasonable that these low He isotopic ratios reflect, in addition to possible long residence times, also the high radiogenic ^4He production in such U-Th-rich lithologies.



5.2 Carbon

The relationship between the TDIC and $\delta^{13}\text{C}_{\text{TDIC}}$ (Figure 5) can provide additional constraints on the sources of fluids. Indeed, deeply rising fluids ascending through the crust interact with rocks and groundwaters that cause changes in carbon abundance and its isotopic composition (Randazzo et al., 2021). From the carbon mass balance approach developed by Chiodini et al. (2000, 2020), we estimate, for each sample, the external carbon contribution, C_{ext} (i.e., the C fractions not resulting from carbonate rock dissolution) and its isotopic composition $\delta^{13}\text{C}_{\text{ext}}$ (see Supplementary Appendix A).

The relationship between C_{ext} and $\delta^{13}\text{C}_{\text{ext}}$ suggests the presence of three distinct carbon sources in the groundwaters (Figure 5). The cold waters fall along the mixing lines (green lines in Figure 5) between a meteoric component ($C_{\text{ext}}= 0.03$ mmol/L; $\delta^{13}\text{C}_{\text{ext}}= -7\%$ to -5.5% ; Apollaro et al., 2020; Chiodini et al., 2011) and a set of end members whose isotopic compositions are in the range of biogenic CO_2 (i.e., $\delta^{13}\text{C}$ from -20% to -28% ; Deines et al., 1974; Hoefs, 2018; Valley and Cole, 2019). We ascribe this component to biogenic (soil) CO_2 dissolving into

groundwaters during their infiltration. Conversely, the samples characterized by more positive $\delta^{13}\text{C}_{\text{ext}}$ values (thermal waters) imply the addition to the shallow CO_2 component with a heavier isotopic signature ($\delta^{13}\text{C}$ of -1‰). This heavy C signature well matches that of deep (crustal/mantle) CO_2 released along the Apennine (Chiodini et al., 2020, 2004). However, also in light of the He isotope evidence previously shown (Figure 3), a major mantle C contribution is very unlikely, and we conclude, therefore, that the thermal waters are dominated by a crustal CO_2 component.

In collisional contexts, large crustal CO_2 fluxes (Becker et al., 2008; Gaillardet and Galy, 2008; Perrier et al., 2009; Evans, 2011; Skelton, 2011; Girault et al., 2014; Menzies et al., 2018; Guo et al., 2021) can be sustained by either regional metamorphism (Groppo et al., 2013; Eberhard and Pettke, 2021) or mechano-chemical CO_2 production (Italiano et al., 2009). Metamorphic processes can operate *via* either 1) decarbonation reactions at relatively high temperatures within calc-silicate rocks (Groppo et al., 2013, 2017, 2020) or 2) dehydration reactions of mineral phases (Eberhard and Pettke, 2021), in which CO_2 degassing is triggered by prograde heating arising from conductive heating triggered by slab breakoff (von Blanckenburg and Davies, 1995), slab rollback (Sizova et al., 2019), or by thermal relaxation of the crust following tectonic thickening upon continent–continent collision. These processes may operate in combination and have certainly interested the past evolution of the Calabrian arc. Notably, metamorphic reactions can have a large CO_2 yield not only where calc-silicate minerals in high-grade rocks and/or limestones are abundant, but also in contexts with relatively few carbonate rocks and/or where siliciclastic metasediments with low carbon contents ($<2\text{ wt\% C}$, Pitcairn et al., 2006) prevail. As aforementioned, the entire study area is made up of important metamorphic complexes (Tursi et al., 2021) that include metabasic rocks, felsic granulites, metapelites, and metacarbonate rocks (Schenk, 1984). The conditions for metamorphic CO_2 production are thus certainly met in the study area. Because such metamorphism occurs at very slow rates, amagmatic CO_2 mobilization along convergent plate boundaries can endure over millions of years (Eberhard and Pettke, 2021).

Considering that the sampled springs fall on major active tectonic discontinuities, responsible for the regional crustal seismicity (Rovida et al., 2019; Rovida et al., 2020; Neri et al., 2006, Neri et al., 2020) and for the circulation and discharge of the thermal waters themselves (Italiano et al., 2010; Apollaro et al., 2012; Vespasiano et al., 2012; Vespasiano et al., 2015a; Tiberti et al., 2017; Apollaro et al., 2019b; Apollaro et al., 2020; Vespasiano et al., 2021), it is likewise possible that mechano-chemical CO_2 production is an additional source for crustal CO_2 , as already proposed for other active seismic areas as Central Apennines (Italiano et al., 2008), eastern Alps (Italiano et al., 2009), and Japan (Nojima fault; Famin et al., 2008).

5.3 $\text{C}/^3\text{He}$ relationship

During their migration and storage in the crust, fluids can undergo different processes that modify their chemical and isotopic compositions. Insights into these processes, and into volatile sources and sinks, can be derived from a joint analysis and interpretation of He and C isotopic signatures (Holland and Gilfillan, 2013; Barry et al., 2020; Randazzo et al., 2021). In order to reconstruct the original signature of deeply sourced fluids, the samples that are dominated by the atmosphere-sourced volatiles (e.g., the cold water) are initially filtered out. Biogenic carbon can be derived from soil or from a deep source as thermal decarboxylation and pyrolysis of organic matter into metapelite ($\delta^{13}\text{C}$ from -30 to -20‰ , Evans et al., 2008). In light of the He isotope evidence, it is reasonable to think that the carbon present in cold waters come from shallow environments (i.e., soil). In fact, carbon from thermal decarboxylation and pyrolysis should be linked to high He concentrations and crustal isotopic signature, while the cold waters are characterized by atmosphere-derived He. Then, we analyze the remaining sample in a $\delta^{13}\text{C}_{\text{ext}}$ vs. $\text{C}_{\text{ext}}/^3\text{He}$ ratio space (Figure 6), in which the potential C–He sources typically plot in distinct compositional fields: mantle and two crustal sources (biogenic vs. crustal-metamorphic) (modified by Sano and Marty, 1995). We find that our samples have $\text{C}_{\text{ext}}/^3\text{He}$ ratios of 4.4×10^9 to 9.1×10^{11} that, coupled with the $\delta^{13}\text{C}_{\text{ext}}$ values, would be consistent with a mixing between crustal-metamorphic ($\text{C}_{\text{ext}}/^3\text{He} = 1 \times 10^{13}$ and $\delta^{13}\text{C}_{\text{ext}} = -3\text{‰}$ to $+3\text{‰}$; Evans et al., 2008; Becker et al., 2008; Dai et al., 1996; Sano and Marty, 1995) and mantle ($\text{CO}_2/^3\text{He} = 2\text{--}4 \times 10^9$ and $\delta^{13}\text{C} = -4\text{‰}$; Marty et al., 2020) fluids in proportions of 88% and 12% (average values; biogenic component would account for 0.8%). However, mantle component fractions (up to 91%) are much higher than calculated above from helium isotopes (2%–3%, Figure 4). This discrepancy can be reconciled taking into account the impact of secondary processes on both $\text{C}_{\text{ext}}/^3\text{He}$ ratios and $\delta^{13}\text{C}_{\text{ext}}$.

5.4 Secondary processes

CO_2 and He have contrasting solubility in water (Ellis and Golding, 1963; Vogel et al., 1970). As such, the two elements undergo selective gas/water partitioning as deeply rising fluids interact with aquifer(s), ultimately altering the $\text{C}_{\text{ext}}/^3\text{He}$ ratio. Carbon isotopes are likewise fractionated during gas–water interactions (Randazzo et al., 2021 and references therein). Thus, both elemental ratios and $\delta^{13}\text{C}$ can be severely modified by secondary processes such as gas dissolution in water and solid-phase (carbonate) precipitation (Gilfillan et al., 2009; Barry and Bekaer, 2021; Randazzo et al., 2021).

We investigated the possible role of secondary processes (e.g., partial gas dissolution in water and calcite precipitation) during

fluid transfer through the crust by modeling (see Gillfillan et al., 2009) their impact on $C_{\text{ext}}/{}^3\text{He}$ ratios and $\delta^{13}\text{C}_{\text{ext}}$ (Figure 6). The process can be modeled as 1) an open-system degassing (Rayleigh-type) at isotopic equilibrium (between phases) and 2) calcite precipitation (Gillfillan et al., 2009). We want to clarify that for a thick crustal sector as Calabrian orogen (thickness up to 38 km; Di Stefano et al., 2009), our model is evidently a simplified approach.

He isotopes indicate a negligible mantle component in thermal waters (up to 2%); hence, the mantle component computed by the C–He relationships (up to 91%) in a simple approach based on mixing between the mantle and crustal end members could be an artefact. Assuming a crustal-metamorphic deep end-member ($C_{\text{ext}}/{}^3\text{He}$ of 1×10^{13} ; Sano and Marty, 1995; O’Nions and Oxburgh, 1988 and $\delta^{13}\text{C}_{\text{ext}}$ of 0.3‰, i.e., the mean value for metamorphic CO_2 ; Becker et al., 2008; Evans et al., 2008; Dai et al., 1996; Figure 6) as pristine gas composition, in order to explain the variability of the $C_{\text{ext}}/{}^3\text{He}$ ratio and $\delta^{13}\text{C}_{\text{ext}}$ in the

samples, we used a two-step model: 1) the partial dissolution of He and CO_2 in groundwater and the progressive variation of the $C_{\text{ext}}/{}^3\text{He}$ ratio and $\delta^{13}\text{C}_{\text{ext}}$ in the residual gas (Figure 6) and 2) the total dissolution of the residual gas (step 1) into a shallow groundwater. The computed model curves show increasing extents of gas dissolution, over a range of pH values at a fixed temperature (30°C mean sample temperature). It is noteworthy that even using different temperatures (from 10 to 40°C), the two models do not show significant differences.

The results of the modeling fit well with the $C_{\text{ext}}/{}^3\text{He}$ ratio and $\delta^{13}\text{C}_{\text{ext}}$ of the thermal waters, suggesting that processes of partial gas dissolution occur at depth. Despite this, we cannot exclude that the lowest $\delta^{13}\text{C}$ values are not at least partially reflecting a biogenic origin (e.g., sample *GdN*), and carbonate precipitation (together with CO_2 dissolution at a lower pH than 5.7–7; Gillfillan et al., 2009) has not taken a role. In light of this, it is plausible to think that the amount of carbon (i.e., CO_2) present below the study area is much more than what we can measure on the surface and that it can be distributed along a multilayer aquifer of which we can only sample the final member. Our model additionally highlights the role played by the gas–water interaction in determining the composition of fluid released in the studied area and also identifies a metamorphic process as a potential source of CO_2 .

5.5 Carbon fluxes

Here, we use the estimated external carbon contributions (C_{ext}) from thermal and cold waters (Figure 5) to constrain the external carbon outflow through the investigated Calabrian groundwater systems. For each site, we combined the spring flow rates with the computed C_{ext} . The so-calculated total C_{ext} flux is $3.63 \times 10^8 \text{ mol year}^{-1}$ of which $4.19 \times 10^7 \text{ mol year}^{-1}$ and $3.21 \times 10^8 \text{ mol year}^{-1}$ from thermal and cold waters, respectively.

For the cold water, we assume that all the C_{ext} is due only to carbon from shallow biogenic sources and atmospheric CO_2 (C_{inf} , i.e., $C_{\text{ext}} = C_{\text{inf}}$). This assumption based on the $\delta^{13}\text{C}_{\text{ext}}$ values is also supported by the presence of atmospheric He dissolved in the cold water, in contrast with the thermal waters that are crustal-He rich (Figures 3, 5). For the thermal waters, the C_{inf} was deconvolved from total C_{ext} (see Supplementary Appendix A). The average C_{inf} of both cold and thermal waters results is $2.5 \pm 1 \text{ mmol/L}$, a value very similar to that estimated for recharge waters of the central-southern Apennines ($2.31 \pm 0.61 \text{ mmol/L}$; Chiodini et al., 2004; Frondini et al., 2019; 2020).

As the deeply derived dissolved carbon (C_{deep}) is given as $C_{\text{ext}} - C_{\text{inf}}$, the deep carbon budget is obtained for each spring by multiplying the dissolved C_{deep} content by the relative water flow rate (see Supplementary Appendix A). The total deep-derived CO_2 output associated with the investigated waters is $2.6 \times 10^7 \text{ mol year}^{-1}$. However, this value is not representative

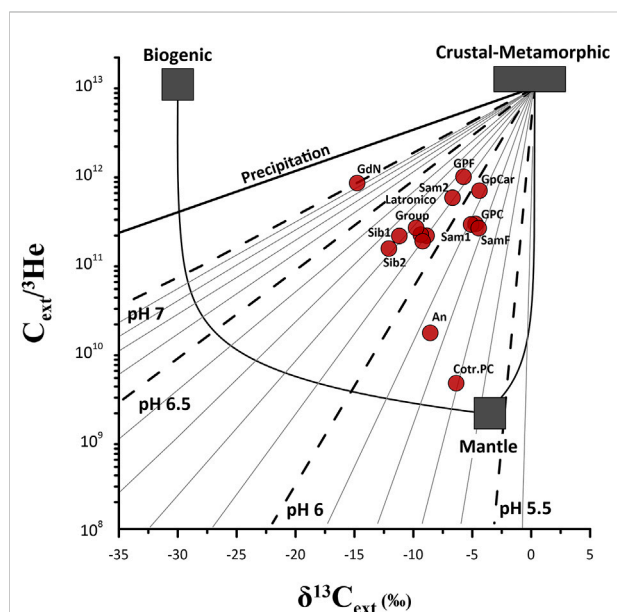


FIGURE 6

Plot of $\delta^{13}\text{C}_{\text{ext}}$ versus $C_{\text{ext}}/{}^3\text{He}$. Changes in $\delta^{13}\text{C}$ are calculated following the method from Gillfillan et al. (2009) using the Rayleigh fractionation equation either for precipitation or for dissolution. In the case of precipitation, there is zero ${}^3\text{He}$ loss from the CO_2 phase and $\text{CO}_2/{}^3\text{He}$ changes in proportion to the fraction of the remaining CO_2 phase, while for CO_2 dissolution, the change in the $\text{CO}_2/{}^3\text{He}$ ratio is calculated following the Rayleigh equation. The gradual loss of CO_2 , with a decrease in the $C_{\text{ext}}/{}^3\text{He}$ ratio and the $\delta^{13}\text{C}$ according with Rayleigh-type gas dissolution at different pHs, is shown from broken lines and slim solid lines, while the predicted trend for carbonate mineral precipitation is from the black solid line. Deep end member with $C_{\text{ext}}/{}^3\text{He} = 1 \times 10^{13}$ (crustal range; Sano and Marty, 1995; O’Nions and Oxburgh, 1988) and $\delta^{13}\text{C}_{\text{ext}}$ from -3 to 3‰ (the mean value of $\delta^{13}\text{C}$ for metamorphic CO_2 is 0.3‰ ; Dai et al., 1996; Hunt et al., 1996; Clark and Fritz, 1997; Evans et al., 2008). The computed model fit nicely the entire dataset with the samples most affected by the secondary processes that also have the highest He concentrations and the lowest values of R/Ra.

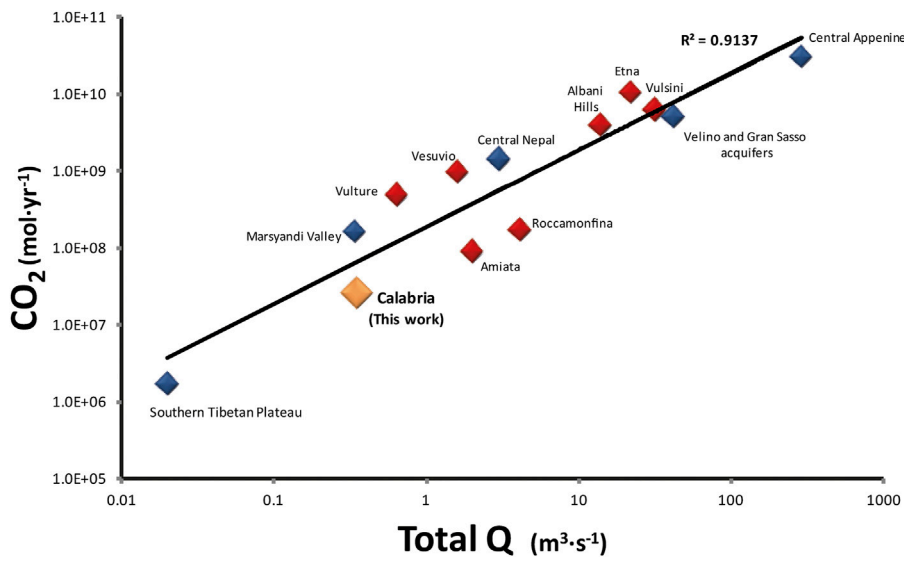


FIGURE 7

CO₂ budget vs. total flow rate for different volcanic and non-volcanic aquifers. The CO₂ budgets are closely related to the flow rates of the investigated springs. The values for CO₂ lost for secondary processes are not included in these budgets. Blue diamonds= non-volcanic area; red diamonds= volcanic area. Data from Caracausi et al. (2015), Becker et al. (2008), Evans et al. (2008), Newell et al. (2008), and Chiodini et al. (2004).

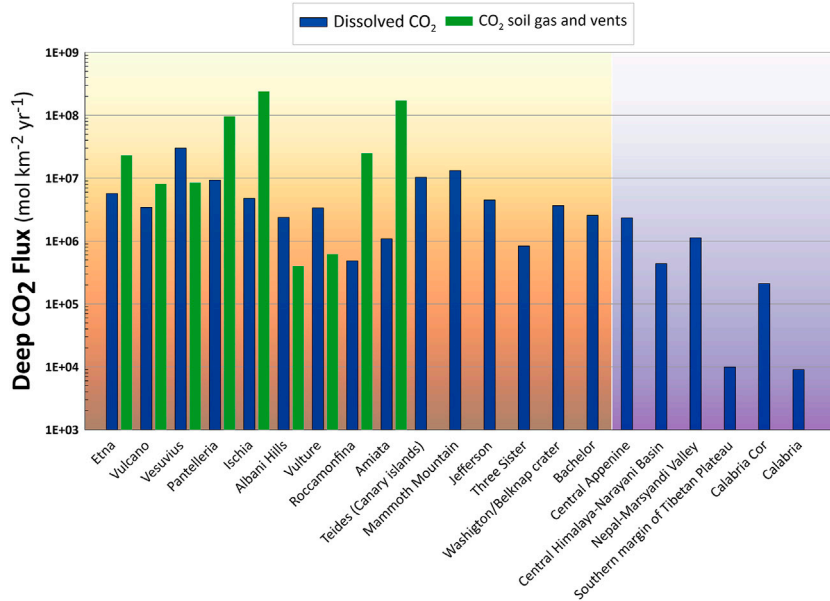


FIGURE 8

Deep CO₂ flux from volcanic and non-volcanic areas. Calabria Cor includes the percentage of deep CO₂ lost for secondary processes (Section 5.4). The Marsyandi Valley and Narayani Basin values refer to total C without extrapolation from biogenic and deep components and included CO₂ lost for degassing processes (Becker et al., 2008; Evans et al., 2008). Orange-yellow background for volcanic areas; purple background for non-volcanic areas. Southern Tibetan Plateau from Newell et al. (2008). Modified after Caracausi et al. (2015).

of the flux from the entire Calabrian orogen and is closely related to the flow rates of the investigated springs as shown by Figure 7.

Therefore, in order to better compare the contribution of deep carbon released from different areas, we also computed the specific flux for each spring, that is, the deep carbon outputs normalized for the catchment areas (see Supplementary Appendix A).

We estimate a value of 2.6×10^7 mol year⁻¹ of deep carbon for the thermal water. Including the percentage of carbon lost due to secondary processes (Section 5.4), we estimate that a value of 6.1×10^8 mol year⁻¹ of deeply derived carbon for an area of 2,880 km² (Supplementary Table S2A) produces a specific flux of 2.1×10^5 mol km⁻² year⁻¹.

This value ranges from two orders of magnitude lower to the same order of CO₂ fluxes defined for some volcanic aquifers (dissolved CO₂ in Figure 8; e.g., Etna 5.7×10^6 mol km⁻² year⁻¹, Vulcano 3.4×10^6 mol km⁻² year⁻¹, Mammoth Mountain 1.7×10^7 mol km⁻² year⁻¹, Mt. Amiata 1.1×10^6 mol km⁻² year⁻¹, Roccamonfina 4.8×10^5 mol km⁻² year⁻¹; Caracausi et al., 2015 and reference therein). Compared with the values from the active tectonic region and collisional orogen (violet gradient background in Figure 8), our result is one order of magnitude lower than that of the deep CO₂ flux estimated for the central Apennine (2.4×10^6 mol km⁻² year⁻¹; Chiodini et al., 2000) and well fitted the range of values estimated for some Himalayan areas. In the latter case, our values are higher than those calculated for the southern margin of the Tibetan Plateau (9.9×10^3 mol km⁻² year⁻¹; Newell et al., 2008), of the same order for the Narayani Basin (4.4×10^5 mol km⁻² year⁻¹; Evans et al., 2008) and one order of magnitude lower than flux values estimated by Becker et al. (2008) for the Marsyandi Valley area (1.1×10^6 mol km⁻² year⁻¹). For the Marsyandi Valley and Narayani basin, the values estimated included the CO₂ lost for degassing processes, but no correction related to the carbon content link to carbonate dissolution or to the biogenic source was made. Therefore, it is probable that the values related to the deep CO₂ are slightly lower. In any case, the values calculated for the Calabria region are comparable to those of areas in which a strong outgassing of CO₂ from a metamorphic source has been identified. We want to clarify that our estimate has many assumptions, and thus an unknown uncertainty, but our intent here is to present a possible limit on CO₂ fluxes for the Calabria region. However, if accurate, our values suggest that the Calabrian orogen is an important contributor to the global carbon budget today.

6 Conclusion

Understanding carbon isotopic signatures and the processes that affect them are critical to make accurate CO₂ flux estimates and identify the origin of carbon. In this study, we investigate the sources and sinks of fluid dissolved in groundwaters from the Pollino and Calabria regions. Chemical and isotopic compositions (He and C) of sampled waters allowed us to

identify two different domains: 1) a shallow system dominated by gas components of the atmospheric signature (He) and biogenic origin (C), and 2) a deeper system in which crustal/deep fluids (CO₂ and He) are dominant.

The external carbon contributions have been calculated following the mass balance approach and coupled with the helium data, which allowed us to identify a deep CO₂ (i.e., crustal/metamorphic) associated with the fluids released in the hydrothermal basins and to detect the secondary process (dissolution/precipitation), which modify the pristine chemical and isotopic compositions of fluids, affecting the deep carbon budget. The samples with the highest He concentrations and the lowest ³He/⁴He ratios also are the most affected by carbon removal processes. This could indicate longer residence time in the crust and/or a more complex circulation system (multilayer) of which the sampled waters are only the last member. We also proposed metamorphic processes as a source of CO₂, but on this, way more studies are required.

For the investigated springs, a total deep-derived CO₂ output of 2.6×10^7 mol year⁻¹ was computed, but the value strongly depends on the flow rates and does not represent the flux from the entire Calabrian orogen. Extrapolating from our model, for the percentage of CO₂ lost due to secondary processes, we estimated a maximum value of 6.1×10^8 mol year⁻¹ for the deeply derived carbon. Scaling our estimate of deep CO₂ flux to the whole study area (2,880 km²), a value of 2.1×10^5 mol km⁻² year⁻¹ is obtained. The value compares to other globally significant carbon fluxes as that defined for the Himalaya orogen and Central Apennine in Italy and despite the considerable uncertainties, represents the first estimate of CO₂ flux for the Calabria region based on the field sampling and modeling of secondary processes facilitating a comparison with estimates from other collisional orogens. Given the extent of flux values extrapolated, we emphasize that more studies should be conducted to implement knowledge on possible sources, circulation systems, and deep CO₂ release by defining the contribution that a collision area such as the Calabrian arc can provide to the global carbon budget.

Data availability statement

The original contributions presented in the study are included in the article/Supplementary Material; further inquiries can be directed to the corresponding author.

Author contributions

PR collected all samples, carried out the analyses, processed the data, and wrote the manuscript. AC helped in sampling and analyses supervision. CA, GV, and MP helped in sampling and analyses. AR helped in sampling. AA and CC helped in

organization and funds. All the authors contributed to the discussion and co-wrote/corrected the manuscript.

Funding

This work was supported by the MIUR project PRIN 2017-2017LMNLAW “Connect4Carbon” and DCO Grant 10881-TDB “Improving the estimation of tectonic carbon flux.”

Conflict of interest

The authors declare that the research was conducted in the absence of any commercial or financial relationships that could be construed as a potential conflict of interest.

References

- Acquafredda, P., Lorenzoni, S., and Zanettin Lorenzoni, E. (1994). Palaeozoic sequences and evolution of the calabrian-peloritan arc (southern Italy). *Terra nova*. 6, 582–594. doi:10.1111/j.1365-3121.1994.tb00525.x
- Aiuppa, A., Fischer, T. P., Plank, T., and Bani, P. (2019). CO₂ flux emissions from the Earth's most actively degassing volcanoes, 2005–2015. *Sci. Rep.* 9, 5442. doi:10.1038/s41598-019-41901-y
- Allocca, V., Celico, F., Celico, P., De Vita, P., Fabbrocino, S., Mattia, S., et al. (2007). Note illustrative della Carta idrogeologica dell'Italia meridionale. [Illustrative notes of the Hydrogeological map of southern Italy]. Istituto Poligrafico e Zecca dello Stato, ISBN 88-448-0215-5 (p. 211), ISBN 88-448-0223-6 (3 maps included)
- Amodio Morelli, L., Bonardi, G., Colonna, V., Dietrich, D., Giunta, G., Ippolito, F., et al. (1976). L'arco calabropeloritano nell'orogene appenninico-magrebide. *Mem. Soc. Geol. It* 17, 1–60.
- Apollaro, C., Bucciantini, A., Vespasiano, G., Varde, M., Fuoco, I., Barca, D., et al. (2019a). Vard'e, M., Fuoco, I., Barca, D., Bloise, A., Miriello, D., Cofone, F., Servidio, A., De Rosa, R. Comparative geochemical study between the tap waters and the bottled mineral waters in Calabria (southern Italy) by compositional data analysis (CoDA) developments. *Appl. Geochem.* 107, 19–33. doi:10.1016/j.apgeochem.2019.05.011
- Apollaro, C., Caracausi, A., Paternoster, M., Randazzo, P., Aiuppa, A., De Rosa, R., et al. (2020). Fluid geochemistry in a low-enthalpy geothermal field along a sector of southern Apennines chain (Italy). *J. Geochem. Explor.* 219, 106618. ISSN 0375-6742. doi:10.1016/j.jgexplo.2020.106618
- Apollaro, C., Dotsika, E., Marini, L., Barca, D., Bloise, A., De Rosa, R., et al. (2012). Chemical and isotopic characterization of the thermo mineral water of Terme Sibarite springs (Northern Calabria, Italy). *Geochem. J.* 46, 117–129. doi:10.2343/geochemj.1.0166
- Apollaro, C., Fuoco, I., Bloise, L., Calabrese, E., Marini, L., Vespasiano, G., et al. 2021. Geochemical modeling of water-rock interaction processes in the Pollino National Park. *Geofluids* 17. doi:10.1155/2021/6655711
- Apollaro, C., Fuoco, I., Brozzo, G., and De Rosa, R. (2019c). Release and fate of Cr (VI) in the ophiolitic aquifers of Italy: The role of Fe (III) as a potential oxidant of Cr (III) supported by reaction path modelling. *Sci. Total Environ.* 660, 1459–1471. doi:10.1016/j.scitotenv.2019.01.103
- Apollaro, C., Tripodi, V., Vespasiano, G., De Rosa, R., Dotsika, E., Fuoco, I., et al. (2019b). Chemical, isotopic and geotectonic relations of the warm and cold waters of the Galatro and Antonimina thermal areas, southern Calabria, Italy. *Mar. Pet. Geol.* 109, 469–483. doi:10.1016/j.marpetgeo.2019.06.020
- Apollaro, C., Vespasiano, G., De Rosa, R., and Marini, L. (2015). Use of mean residence time and flowrate of thermal waters to evaluate the volume of reservoir water contributing to the natural discharge and the related geothermal reservoir volume. Application to Northern Thailand hot springs. *Geothermics* 58, 62–74. doi:10.1016/j.geothermics.2015.09.0062015
- Apollaro, C., Vespasiano, G., Muto, F., De Rosa, R., Barca, D., and Marini, L. (2016). Use of mean residence time of water, flowrate, and equilibrium temperature

Publisher's note

All claims expressed in this article are solely those of the authors and do not necessarily represent those of their affiliated organizations, or those of the publisher, the editors, and the reviewers. Any product that may be evaluated in this article, or claim that may be made by its manufacturer, is not guaranteed or endorsed by the publisher.

Supplementary material

The Supplementary Material for this article can be found online at: <https://www.frontiersin.org/articles/10.3389/feart.2022.946707/full#supplementary-material>

indicated by water geothermometers to rank geothermal resources. Application to the thermal water circuits of Northern Calabria. *J. Volcanol. Geotherm. Res.* 328, 147–158. doi:10.1016/j.jvolgeores.2016.10.014

Atzori, P., Ferla, P., Paglionico, A., Piccarreta, G., and Rottura, A. (1984). Remnants of the hercynian orogen along the “calabrian-peloritan arc”, southern Italy: A review. *J. Geol. Soc. Lond.* 141, 137–145. doi:10.1144/gsjgs.141.1.0137

Ballentine, C. J., and Burnard, P. (2002). Production, release and transport of noble gases in the continental crust. *Rev. Mineralogy Geochem.* 47 (1), 481–538. doi:10.2138/rmg.2002.47.12

Barnes, I., Irwin, P. W., and White, D. E. Global distribution of carbon dioxide discharges, and major zones of seismicity. *Water resour. Invest. WRI 78–39* (U.S. Geol. Surv., Washington, DC, 1978).

Barry, P. H., Bekaer, D. V., Halldorsson, S. A., de Moor, J., et al. (2021). Helium-carbon systematics of groundwaters in the lassin peak region. *Chem. Geol.* 584, 120535. ISSN 0009-2541. doi:10.1016/j.chemgeo.2021.120535

Barry, P. H., Negrete-Aranda, R., Spelz, R. M., Seltzer, A. M., Bekaert, D. V., Virrueta, C., et al. (2020). Volatile sources, sinks and pathways: A helium-carbon isotope study of baja California fluids and gases. *Chem. Geol.* 550, 119722. doi:10.1016/j.chemgeo.2020.119722

Beccaluva, L., Chiesa, S., and Delaloye, M. (1981). K/Ar age determinations on some Tethyan ophiolites. *Rend. Soc. Ital. Mineral. Pet.* 37, 869–880.

Becker, J. A., Bickle, M. J., Galy, A., and Holland, T. J. B. (2008). Himalayan metamorphic CO₂ fluxes: Quantitative constraints from hydrothermal springs. *Earth Planet. Sci. Lett.* 265, 616–629. doi:10.1016/j.epsl.2007.10.046

Bencini, A., and Ciraco, G. (1982). Caratteristiche geochemiche di alcune acque termali della provincia di Catanzaro. *Rendiconti Simp.* 38, 1189–1195.

Berner, R. A., and Lagasa, A. C. (1989). Modeling the geochemical carbon cycle. *Sci. Am.* 260, 74–81. doi:10.1038/scientificamerican0389-74

Borsi, S., and Dubois, R. (1968). Données géochronologiques sur l'histoire hercynienne et Alpine de la Calabre Centrale. *C. R. Acad. Sci. Ser. D.* 266, 72–75.

Boschi, E., Guidoboni, E., Ferrari, G., Mariotti, D., Valensise, G., and Gasperini, P. (2000). Catalogue of strong Italian earthquakes, 461 B.C. to 1997. *Ann. Geofis.* 43, 609–868. (with database on CD-ROM). doi:10.4401/ag-3668

Brutto, F., Muto, F., Loreto, M. F., De Paola, N., Tripodi, V., Critelli, S., et al. (2016). The neogene-quaternary geodynamic evolution of the central Calabrian arc: A case study from the Western Catanzaro Trough basin. *J. Geodyn.* 102, 95–114. doi:10.1016/j.jog.2016.09.002

Burton, M. R., Sawyer, G. M., and Granieri, D. (2013). Deep carbon emissions from volca-noes. *Rev. Mineral. Geochem.* 75, 323–354. doi:10.2138/rmg.2013.75.11

Calcara, M., and Quattrocchi, F. 1993. Sulla scelta di Siti idonei al Monitoraggio geochemico ai fini della sorveglianza sismica della Calabria settentrionale: Valle Crati/ piana di Sibari. Atti convegno nazionale GNGTS.

- Capasso, G., Favara, R., Grassa, F., Inguaggiato, S., and Longo, M. (2005). On-line technique for preparing and measuring stable carbon isotope of total dissolved inorganic carbon in water samples ($\delta^{13}\text{C}_{\text{DIC}}$). *Ann. Geophys.* 48, 159–166. doi:10.4401/ag-3190
- Capasso, G., and Inguaggiato, S. (1998). A simple method for the determination of dissolved gases in natural waters: An application to the thermal waters from Volcano Island. *Appl. Geochem.* 13, 631–642. doi:10.1016/S0883-2927(97)00109-1
- Caracausi, A., Paternoster, M., and Nuccio, P. M. (2015). Mantle CO₂ degassing at Mt. Vulture volcano (Italy): Relationship between CO₂ outgassing of volcanoes and the time of their last eruption. *Earth Planet. Sci. Lett.* 411, 268–280. doi:10.1016/j.epsl.2014.11.049
- Caracausi, A., and Sulli, A. (2019). Outgassing of mantle volatiles in compressional tectonic regime away from volcanism: The role of continental delamination. *Geochem. Geophys. Geosyst.* 20, 2007–2020. doi:10.1029/2018GC008046
- Castello, B., Selvaggi, G., Chiarabba, C., and Amato, A. (2006). CSI, Catalogo della sismicità italiana 1981–2002, versione 1.1, INGV-CNT Roma. Available at: <http://www.ingv.it/CSI/>.
- Catalano, S., De Guidi, G., Monaco, C., Tortorici, G., and Tortorici, L. (2008). Active faulting and seismicity along the siculo-calabrian rift zone (southern Italy). *Tectonophysics* 453, 177–192. doi:10.1016/j.tecto.2007.05.008
- Chiarabba, C., De Gpri, P., and Speranza, F. (2008). - the southern Tyrrhenian subduction zone. *Deep geometry, magmatism Plio-Pleistocen EEarth Planet. Sci. Lett* 268, 408–423. doi:10.1016/j.epsl.2008.01.036
- Chiarella, D., Longhitano, S. G., and Muto, F. (2012). Sedimentary features of the Lower Pleistocene mixed siliciclastic-bioclastic tidal deposits of the Catanzaro Strait (Calabrian Arc, south Italy). *Rend. Online Soc. Geol. Ital.* 21, 919–920.
- Chiarella, D., Moretti, M., Longhitano, S. G., and Muto, F. (2016). Deformed cross-stratified deposits in the early Pleistocene tidally-dominated Catanzaro Strait-fill succession, Calabrian arc (southern Italy): Triggering mechanisms and environmental significance. *Sediment. Geol.* 344, 277–289. doi:10.1016/j.sedgeo.2016.05.003
- Chiodini, G., Caliro, A., Cardellini, C., Frondini, F., Inguaggiato, S., and Matteucci, F. (2011). Inguaggiato S. & Matteucci F- *Geochemical evidence for and characterization of CO₂ rich gas sources in the epicentral area of the Abruzzo 2009 earthquakes.* *Earth Planet. Sci. Lett.* 304, 389–398. doi:10.1016/j.epsl.2011.02.016
- Chiodini, G., Cardellini, C., Amato, A., Boschi, E., Caliro, S., Frondini, F., et al. (2004). - *Carbon dioxide Earth degassing and seismogenesis in central and southern Italy.* *Geophys. Res. Lett.* 31, L07615.
- Chiodini, G., Cardellini, C., Di Luccio, F., Selva, J., Frondini, F., Caliro, S., et al. (2020). Correlation between tectonic CO₂ Earth degassing and seismicity is revealed by a 10-year record in the Apennines. *Italy. Sci. Adv.* 6, eabc2938
- Chiodini, G., Frondini, F., Cardellini, C., Parello, F., and Peruzzi, L. (2000). Rate of diffuse carbon dioxide Earth degassing estimated from carbon balance of regional aquifers: The case of central Apennine, Italy. *J. Geophys. Res.* 105, 8423–8434. doi:10.1029/1999jb900355
- Cirriacione, R., Fazio, E., Fiannacca, P., Ortolano, G., Pezzino, A., and Punturo, R. (2015). The Calabria-Peloritani Orogen, a composite terrane in Central Mediterranean; its overall architecture and geodynamic significance for a pre-Alpine scenario around the Tethyan basin. *Progresses in Deciphering Structures and Compositions of Basement Rocks.* *Period. Mineral* 84, 701–749. doi:10.2451/2015PM0446
- Cirriacione, R., Ortolano, G., Pezzino, A., and Punturo, R. (2008). Poly-orogenic multi-stage metamorphic evolution inferred via P-T pseudosections: An example from Aspromonte Massif basement rocks (Southern Calabria, Italy). *Lithos* 103 (3–4), 466–502. <https://doi.org/10.1016/j.lithos.2007.11.001>
- Clark, I. D., and Fritz, P. (1997). environmental isotopes in hydrogeology CRC press/lewis publishers. Boca Raton, 328.
- Dai, J., Song, Y., Dai, C., and Wang, D. (1996). Geochemistry and accumulation of carbon dioxide gases in China. *AAPG Bull.* 80 (10), 1615–1625. doi:10.1306/64EDA0D2-1724-11D7-8645000102C1865D
- Dasgupta, R. (2013). Ingassing, storage, and outgassing of terrestrial carbon through geologic time. *Rev. Mineralogy Geochem.* 75 (1), 183–229. doi:10.2138/rmg.2013.75.7
- De Matteis, R., Convertito, V., Napolitano, F., Amoroso, O., Terakawa, T., and Capuano, P. (2021). Pore fluid pressure imaging of the Mt. Pollino region (southern Italy) from earthquake focal mechanisms. *Geophys. Res. Lett.* 48, e2021GL094552. doi:10.1029/2021GL094552
- De Vita, P., Allocca, V., Celico, F., Fabbrocino, S., Mattia, C., Monacelli, G., et al. (2018). Hydrogeology of continental southern Italy. *J. Maps* 14 (2), 230–241. doi:10.1080/17445647.2018.1454352
- Deines, P., Langmuir, D., and Harmon, R. S. (1974). Stable carbon isotope ratios and the existence of a gas phase in the evolution of carbonate ground waters. *Geochimica Cosmochimica Acta* 38 (7), 1147–1164. ISSN 0016-7037. doi:10.1016/0016-7037(74)90010-6
- Del Moro, A., Paglionico, A., Piccarreta, G., and Rottura, A. (1986). Tectonic structure and post-hercynian evolution of the serre, Calabrian arc, southern Italy: Geological, petrological and radiometric evidences. *Tectonophysics* 124, 223–238. doi:10.1016/0040-1951(86)90202-7
- Devoti, R., Riguzzi, F., Cuffaro, M., and Doglioni, C. (2008). New GPS constraints on the kinematics of the Apennines subduction. *Earth Planet. Sci. Lett.* 273, 163–174. doi:10.1016/j.epsl.2008.06.031
- Di Stefano, R., Kissling, E., Chiarabba, C., Amato, A., and Giardini, D. (2009). Shallow subduction beneath Italy: Three-dimensional images of the Adriatic-European-Tyrrhenian lithosphere system based on high-quality P wave arrival times. *J. Geophys. Res.* 114, B05305. doi:10.1029/2008jb005641
- Dichicco, M. C., Paternoster, M., Rizzo, G., and Sinisi, R. (2019). Mineralogical asbestos assessment in the southern apennines (Italy): A review. *Fibers* 2019 (7), 24. doi:10.3390/fib7030024
- Duchi, V., Bencini, A., Cortese, G., and Minissale, A. (1991). Caratteristiche geochimiche dei fluidi della Calabria centro settentrionale e loro potenzialità geotermiche. *Boll. Soc. Geol. It* 110, 273–280.
- Dumas, B., and Raffy, J. (2004). Late Pleistocene tectonic activity deduced from uplifted marine terraces in Calabria, facing the Strait of Messina. *Quat. nuova* VIII, 79–99.
- Eberhard, L., and Pettko, T. (2021). Antigorite dehydration fluids boost carbonate mobilisation and crustal CO₂ outgassing in collisional orogens. *Geochimica Cosmochimica Acta* 300, 192–214. ISSN 0016-7037. doi:10.1016/j.gca.2021.02.030
- Ellis, A. J., and Golding, R. M. (1963). The solubility of carbon dioxide above 100 degrees C in water and in sodium chloride solutions. *Am. J. Sci.* 261, 47–60. doi:10.2475/ajs.261.1.47
- Evans, K. (2011). Metamorphic carbon fluxes: How much and how fast? *Geology* 39 (1), 95–96. doi:10.1130/focus012011.110.1130/focus012011.1
- Evans, M. J., Derry, L. A., and France-Lanord, C. (2008). Degassing of metamorphic carbon dioxide from the Nepal Himalaya. *Geochem. Geophys. Geosyst.* 9Q04021. doi:10.1029/2007GC001796
- Faccenna, C., Becker, T. W., Lucente, F. P., Jolivet, L., and Rossetti, F. (2001). History of subduction and back-arc extension in the central Mediterranean. *Geophys. J. Int.* 145, 809–820. doi:10.1046/j.0956-540x.2001.01435.x
- Faccenna, C., Molin, P., Orecchio, B., Olivetti, V., Bellier, O., Funicello, F., et al. (2011). Topography of the Calabria subduction zone (southern Italy): Clues for the origin of Mt. Etna. *Tectonics* 30, 2010TC002694. doi:10.1029/2010tc002694
- Famin, V., Nakashima, S., Boullier, A., Fujimoto, K., and Hirono, T. (2008). Earthquakes produce carbon dioxide in crustal faults. *Earth Planet. Sci. Lett.* 265, 487–497. ISSN 0012-821X. doi:10.1016/j.epsl.2007.10.041
- Ferranti, L., Monaco, C., Morelli, D., Antonioli, F., and Maschio, L. (2008). Holocene activity of the scilla fault, southern Calabria: Insights from coastal morphological and structural investigations. *Tectonophysics* 453, 74–93. doi:10.1016/j.tecto.2007.05.006
- Fischer, T. P. (2013). DEep Carbon DEgassing: The deep carbon observatory DECADE initiative. *Mineral. Mag.* 77 (5), 1089.
- Fischer, T. P., and Aiuppa, A. (2020). AGU centennial grand challenge: Volcanoes and deep carbon global CO₂ emissions from subaerial volcanism—recent progress and future challenges. *Geochem. Geophys. Geosyst.* 21, e2019GC008690. doi:10.1029/2019GC008690
- Fischer, T. P., Arellano, S., Carn, S., Aiuppa, A., Galle, B., Allard, P., et al. (2019). The emissions of CO₂ and other volatiles from the world's subaerial volcanoes. *Sci. Rep.* 9 (1), 18716. doi:10.1038/s41598-019-54682-1
- Foster, G., Royer, D., and Lunt, D. (2017). Future climate forcing potentially without precedent in the last 420 million years. *Nat. Commun.* 8, 14845. doi:10.1038/ncomms14845
- Frondini, F., Cardellini, C., Caliro, S., Beddini, G., and Rosiello, A. (2019). Measuring and interpreting CO₂ fluxes at regional scale: The case of the apennines, Italy. *J. Geol. Soc. Lond.* 176 (2), 408–416. doi:10.1144/jgs2017-169
- Guo, Z., Wilson, M., Dingwell, D. B., and Liu, J. (2021). India-Asia collision as a driver of atmospheric CO₂ in the Cenozoic. *Nat. Commun.* 12, 3891. doi:10.1038/s41467-021-23772-y
- Gaillardet, J., and Galy, A. (2008). *Science* 320, 1727–1728. doi:10.1126/science.1159279
- Gilfillan, S. M. V., Lollar, B. S., Holland, G., Blagburn, D., Stevens, S., Schoell, M., et al. (2009). Solubility trapping in formation water as dominant CO₂ sink in natural gas fields. *Nature* 458 (7238), 614–618. doi:10.1038/nature07852

- Girault, F., Perrier, F., Crockett, R., Bhattarai, M., Koirala, B. P., France-Lanord, C., et al. (2014). The syabru-bensi hydrothermal system in central Nepal: 1. Characterization of carbon dioxide and radon fluxes. The syabru-bensi hydrothermal system in central Nepal: 1. Characterization of carbon dioxide and radon fluxes. *Journal of geophysical research: J. Geophys. Res. Solid Earth* 119, 4017–4055. doi:10.1002/2013jb010301
- Graessner, T., and Schenk, V. (2001). An exposed Hercynian deep crustal section in the Sila Massif of Northern Calabria: Mineral chemistry, petrology and a P-T path of granulite-facies metapelitic migmatites and metabasites. *J. Petrology* 42 (5), 931–961. doi:10.1093/petrology/42.5.931
- Groppo, C., Rapa, G., Frezzotti, M. L., and Rolfo, F. (2020) The fate of calcareous pelites in collisional orogens. *J. Metamorph. Geol.* doi:10.1111/jmg.12568
- Groppo, C., Rolfo, F., Castelli, D., and Connolly, J. A. D. (2013). - *Metamorphic CO2 production from calc-silicate rocks via garnet-forming reactions in the CFAS-H2O-CO2 system. Contrib. Mineral. Pet.* 166, 1655–1675. doi:10.1007/s00410-013-0947-5
- Groppo, C., Rolfo, F., and Frezzotti, M. L. (2022). CO₂ outgassing during collisional orogeny is facilitated by the generation of immiscible fluids. *Commun. Earth Environ.* 3, 13. doi:10.1038/s43247-022-00340-w
- Groppo, C., Rolfo, F., Mosca, P., and Castelli, D. (2017) - *metamorphic CO2 production in collisional orogens: Petrologic constraints from phase diagram modeling of himalayan, scapolite-bearing, calc-silicate rocks in the NK(C,F)MAS(T)-HC system. Journal of petrology.* doi:10.1093/petrology/egx005
- Gruppo di lavoro CPTI (2004). Bologna. <http://emidius.mi.ingv.it/CPTI04>. Catalogo parametrico dei terremoti italiani, versione 2004 (CPTI04), INGV
- Gurrieri, S., Hauser, S., and Valenza, M. (1984). Indagine preliminare su alcune sorgenti termali della Calabria per una futura sorveglianza geochemica dell'attività sismica. *Min. Petrog. Acta* 28, 101–122.
- Hoefs, J. (2018). "Variations of stable isotope ratios in nature," in *Stable isotope geochemistry*. Editor J. Hoefs (Springer), 229–432.
- Holland, G., and Gilfillan, S. (2013), *Application of noble gases to the viability of CO2 storage. in The noble gases as geochemical tracers. Advances in isotope geochemistry.* Editor P. Burnard (Springer), 177–223. doi:10.1007/978-3-642-28836-4
- Hollenstein, C., Kahle, H. G., Geiger, A., Jenny, S., Goes, S., and Giardini, D. (2003). New GPS constraints on the Africa-Eurasia plate boundary zone in southern Italy. *Geophys. Res. Lett.* 30 (18), 1935. doi:10.1029/2003gl017554
- Hunt, H. W., Elliott, E. T., Detling, J. K., Morgan, J. A., and Chen, D.-X. (1996). Responses of a C₃ and a C₄ perennial grass to elevated CO₂ and temperature under different water regimes. *Glob. Chang. Biol.* 2, 35–47. doi:10.1111/j.1365-2486.1996.tb00047.x
- Iannace, A., Vitale, S., D'errico, M., Mazzoli, S., Di Staso, A., Macaione, E., et al. (2007). Di staso, A., macaione, E., Messina A., redde S.M., somma R., zamparelli V., zattin M. and Bonardi, G. The carbonate tectonic units of northern Calabria (Italy): A record of apulian palaeomargin evolution and Miocene convergence, continental crust subduction, and exhumation of HP-LT rocks. *J. Geol. Soc. Lond.* 164 (6), 1165–1186. doi:10.1144/0016-76492007-0171165-1186
- Inguaggiato, S., and Rizzo, A. (2004). Dissolved helium isotope ratios in groundwaters: A new technique based on gas–water re-equilibration and its application to stromboli volcanic system. *Appl. Geochem.* 19, 665–673. doi:10.1016/j.apgeochem.2003.10.009
- Italiano, F., Bonfanti, P., Ditta, M., Petrini, R., and Slejko, F., Helium and carbon isotopes in the dissolved gases of Friuli Region (NE Italy): Geochemical evidence of CO₂ production and degassing over a seismically active area. *Chem. Geol.*, 266, Issues 76–85, 2009, Pages 76–85, ISSN 0009-2541, doi:10.1016/j.chemgeo.2009.05.022
- Italiano, F., Bonfanti, P., Pizzino, L., and Quattrocchi, F. (2010). Geochemistry of fluids discharged over the seismic area of the southern apennines (Calabria region, southern Italy): Implications for fluid-fault relationships. *Appl. Geochem.* 25, 540–554. doi:10.1016/j.apgeochem.2010.01.011
- Italiano, F., Martinelli, G., and Plescia, P. (2008). CO₂ degassing over seismic areas: The role of mechanochemical production at the study case of central apennines. *Pure Appl. Geophys.* 165, 75–94. doi:10.1007/s00024-007-0291-7
- Jolivet, L., and Faccenna, C. (2000). Mediterranean extension and the Africa-Eurasia collision. *Tectonics* 19 (6), 1095–1106. doi:10.1029/2000tc900018
- Kerrick, D. M. (2001). Present and past nonanthropogenic CO₂ degassing from the solid Earth. *Rev. Geophys.* 39, 565–585. doi:10.1029/2001rg000105
- Lee, C.-T., Jiang, H., Dasgupta, R., and Torres, M. (2019). "A framework for understanding whole-Earth carbon cycling" in *Deep carbon: Past to present*. Editors B. N. Orcutt, I. Daniel, and R. Dasgupta (Cambridge: Cambridge University Press), 313–357.
- Lee, H., Muirhead, J. D., Fischer, T. P., Ebinger, C. J., Kattenhorn, S. A., Sharp, Z. D., et al. (2016). Massive and prolonged deep carbon emissions associated with continental rifting. *Nat. Geosci.* 9, 145–149. doi:10.1038/ngeo2622
- Liberi, F., Morten, L., and Piluso, E. (2006). Geodynamic significance of ophiolites within the Calabrian arc. *Isl. Arc* 15 (1), 26–43. doi:10.1111/j.1440-1738.2006.00520.x
- Liberi, F., Piluso, E., and Langone, A. (2011). Permo-Triassic thermal events in the lower Variscan continental crust section of the Northern Calabrian Arc, Southern Italy: Insights from petrological data and *in situ* U-Pb zircon geochronology on gabbros. *Lithos* 124 (3–4), 291–307. doi:10.1016/j.lithos.2011.02.016
- Liu, J., and Han, G. (2020). Effects of chemical weathering and CO₂ outgassing on δ¹³C_{DIC} signals in a karst watershed. *J. Hydrology* 589, 125192. doi:10.1016/j.jhydrol.2020.125192ISSN 0022-1694
- Longhitano, S. G., Chiarella, D., and Muto, F. (2014). Three-dimensional to two-dimensional cross-strata transition in the lower Pleistocene Catanzaro tidal strait transgressive succession (southern Italy). *Sedimentology* 61, 2136–2171. doi:10.1111/sed.12138
- Lucente, F. P., Chiarabba, C., Cimini, G. B., and Giardini, D. (1999). Tomographic constraints on the geodynamic evolution of the Italian region. *J. Geophys. Res.* 104 (B9), 20307–20327. doi:10.1029/1999jb900147
- Malinverno, A., and Ryan, W. B. F. (1986). Extension in the Tyrrhenian Sea and shortening in the Apennines as result of arc migration driven by sinking of the lithosphere. *Tectonics* 5, 227–245. doi:10.1029/tc005i002p00227
- Margiotta, S., Mongelli, G., Paternoster, M., Sinisi, R., and Summa, V. (2014). Seasonal groundwater monitoring for trace-elements distribution and Cr(VI) pollution in an area affected by negligible anthropogenic effects. *Fresen Environ. Bull.* 23, 1–15.
- Margiotta, S., Mongelli, G., Summa, V., Paternoster, M., and Fiore, S. (2012). Trace element distribution and Cr(VI) speciation in Ca-HCO₃ and Mg-HCO₃ spring waters from the northern sector of the Pollino massif, southern Italy. *J. Geochem. Explor.* 115, 1–12. doi:10.1016/j.jexplo.2012.01.006
- Marty, B., Almayrac, M., Barry, P. H., Bekaert, D. V., Broadley, M. W., Byrne, D. J., et al. (2020). An evaluation of the C/N ratio of the mantle from natural CO₂-rich gas analysis: Geochemical and cosmochemical implications. *Earth Planet. Sci. Lett.* 551 (2020), 116574. doi:10.1016/j.epsl.2020.116574
- Menzies, C. D., Wright, S. L., Craw, D., James, R. H., Alt, J. C., Cox, S. C., et al. (2018). Carbon dioxide generation and drawdown during active orogenesis of siliciclastic rocks in the Southern Alps, New Zealand. *Earth Planet. Sci. Lett.* 481, 305–315. ISSN 0012-821X. doi:10.1016/j.epsl.2017.10.010
- Messina, A., Russo, S., Borghi, A., Colonna, V., Compagnoni, R., Caggianelli, A., et al. (1994). Il massiccio della Sila settore settentrionale dell'Arco calabro-peloritano. *Boll. Soc. Geol. It.* 113, 539–586.
- Micheletti, F., Barbey, P., Fornelli, A., Piccarreta, G., and Deloué, E. (2007). Latest Precambrian to Early Cambrian U–Pb zircon ages of augen gneisses from Calabria (Italy), with inference to the Alboran microplate in the evolution of the peri-Gondwana terranes. *Int. J. Earth Sci.* 96, 843–860. doi:10.1007/s00531-006-0136-0
- Minissale, A. (2004). Origin, transport and discharge of CO₂ in central Italy. *Earth. Sci. Rev.* 66, 89–141. doi:10.1016/j.earscirev.2003.09.001
- Monaco, C., Tortorici, L., Nicolich, R., Cernobori, L., and Costa, M. (1996). From collisional to rifted basins: An example from the southern Calabrian Arc (Italy). *Tectonophysics* 266 (1–4), 233–249. doi:10.1016/s0040-1951(96)00192-8
- Napolitano, F., Galluzzo, D., Gervasi, A., Scarpa, R., and La Rocca, M. (2021). Fault imaging at Mt Pollino (Italy) from relative location of microearthquakes. *Geophys. J. Int.* 224 (1), 637–648. doi:10.1093/gji/ggaa407
- Neri, G., Barberi, G., Oliva, G., Orecchio, B., and Presti, D. (2006). A possible seismic gap within a highly seismogenic belt crossing Calabria and eastern sicily, Italy. *Bull. Seismol. Soc. Am.* 96, 1321–1331. doi:10.1785/0120050170
- Neri, G., Marotta, A. M., Orecchio, B., Presti, D., Totaro, C., Barzaghi, R., et al. (2012). How lithospheric subduction changes along the Calabrian arc in southern Italy: Geophysical evidences. *Int. J. Earth Sci.* 101, 1949–1969. doi:10.1007/s00531-012-0762-7
- Neri, G., Orecchio, B., Scolaro, S., and Totaro, C. (2020). Major earthquakes of southern Calabria, Italy, into the regional geodynamic context. *Front. Earth Sci.* 8, 579846. doi:10.3389/feart.2020.579846
- Neri, G., Orecchio, B., Totaro, C., Falcone, G., and Presti, D. (2009). Subduction beneath southern Italy close the ending: Results from seismic tomography. *Seismol. Res. Lett.* 80 (1), 63–70. doi:10.1785/gssrl.80.1.63
- Newell, D. L., Jessup, M. J., Cottle, J. M., Hilton, D. R., Sharp, Z. D., and Fischer, T. P. (2008). Aqueous and isotope geochemistry of mineral springs along the southern margin of the Tibetan plateau: Implications for fluid sources and regional degassing of CO₂. *Geochem. Geophys. Geosyst.* 9, Q08014, doi:10.1029/2008GC002021
- Nocquet, J.-M. (2012). Present-day kinematics of the mediterranean: A comprehensive overview of GPS results. *Tectonophysics* 579, 220–242. doi:10.1016/j.tecto.2012.03.037

- O'Nions, R. K., and Oxburgh, E. R. (1988). Helium, volatile fluxes and the development of continental crust. *Earth Planet. Sci. Lett.* 90 (3), 331–347. doi:10.1016/0012-821X(88)90134-3
- Ogniben, L. (1969). Schema introduttivo alla geologia del confine Calabro-lucano. *Mem. Soc. Geol. It* 8, 453–763.
- Ortolano, G., Visalli, R., Fazio, E., Fiannacca, P., Godard, G., Pezzino, A., et al. (2020). Tectono-metamorphic evolution of the Calabria continental lower crust: The case of the Sila Piccola Massif. *Int. J. Earth Sci.* 109, 1295–1319. doi:10.1007/s00531-020-01873-1
- Ozima, M., and Podosek, F. A. (2002). *Noble gas geochemistry*. Cambridge University Press, 286.
- Parkhurst, D. L., and Appelo, C. A. J. 1999. User's guide to PHREEQC a computer program for speciation, reaction-path, 1D-transport, and inverse geochemical calculations (Version 2). Technical Report 99-4259. U. S. Geological Survey, USA.
- Pastori, M., Margheriti, L., De Gori, P., Govoni, A., Lucente, F. P., Moretti, M., et al. (2021). The 2011–2014 Pollino seismic swarm: Complex fault systems imaged by 1D refined location and shear wave splitting analysis at the apennines–Calabrian arc boundary. *Front. Earth Sci.* 9, 618293. doi:10.3389/feart.2021.618293
- Paternoster, M., Rizzo, G., Sinisi, R., Vilaridi, G., Di Palma, L., and Mongelli, G. (2021). Natural hexavalent chromium in the Pollino massif groundwater (southern apennines, Italy): Occurrence, geochemistry and preliminary remediation tests by means of innovative adsorbent nanomaterials. *Bull. Environ. Contam. Toxicol.* 106, 421–427. doi:10.1007/s00128-020-02898-7
- Perrier, F., Richon, P., Byrdina, S., France-Lanord, C., Rajaura, S., Koirala, B. P., et al. (2009). A direct evidence for high carbon dioxide and radon-222 discharge in Central Nepal. *Earth Planet. Sci. Lett.* 278, 198–207. doi:10.1016/j.epsl.2008.12.008
- Piana Agostinetti, N., Steckler, M. S., and Lucente, F. P. (2009). Imaging the subducted slab under the Calabrian Arc, Italy, from receiver function analysis. *Lithosphere* 1 (3), 131–138. doi:10.1130/L49.1
- Piccarreta, G. (1981). Deep-rooted overthrusting and blueschistic metamorphism in compressive continental margins. An example from Calabria (Southern Italy). *Geol. Mag.* 118 (5), 539–544. doi:10.1017/S0016756800032908
- Pitcairn, I. K., Teagle, D. A. H., Craw, D., Olivio, G. R., Kerrich, R., and Brewer, T. S. (2006). Sources of metals and fluids in orogenic gold deposits: Insights from the otago and alpine schists, New Zealand. *Econ. Geol.* 101, 1525–1546. doi:10.2113/gsecongeo.101.8.1525
- Randazzo, P., Caracausi, A., Aiuppa, A., Cardellini, C., Chiodini, G., D'Alessandro, W., et al. (2021). Active degassing of deeply sourced fluids in central Europe: New evidences from a geochemical study in Serbia. *Geochem. Geophys. Geosyst.* 22, e2021GC010017. doi:10.1029/2021GC010017
- Rizzo, A. L., Caracausi, A., Chavagnac, V., Nomikou, P., Polymenakou, P. N., Mandalakis, M., et al. (2019). Geochemistry of CO₂-rich gases venting from submarine volcanism: The case of kolumbo (hellenic volcanic arc, Greece). *Front. Earth Sci.* 7, 1–20. doi:10.3389/feart.2019.00060
- Rolfo, F., Groppo, C., and Mosca, P. (2015). Metamorphic CO₂ production in calc-silicate rocks from the eastern Himalaya. *Italian Journal of Geosciences*. 136 (1), 28–38. doi:10.3301/IJG.36
- Rossetti, F., Faccenna, C., Goffe, B., Monie, P., Argentieri, A., Funicello, R., et al. (2001). Alpine structural and metamorphic signature of the Sila piccola massif nappe stack (Calabria, Italy): Insights for the tectonic evolution of the Calabrian arc. *Tectonics* 20 (1), 112–133. doi:10.1029/2000tc900027
- Rossetti, F., Goffe, B., Monie, P., Faccenna, C., and Vignaroli, G. (2004). Alpine orogenic P-T-t-deformation history of the Catena Costiera area and surrounding regions (Calabrian Arc, southern Italy): The nappe edifice of north Calabria revised with insights on the Tyrrhenian-Apennine system formation. *Tectonics* 23 (6), 1–26. doi:10.1029/2003tc001560
- A. Rovida, M. Locati, R. Camassi, B. Lolli, and P. Gasperini (Editors) (2016). *CPTI15, the 2015 version of the Parametric Catalogue of Italian Earthquakes*. Istituto Nazionale di Geofisica e Vulcanologia. doi:10.6092/INGV.IT-CPTI15
- Rovida, A., Locati, M., Camassi, R., Lolli, B., and Gasperini, P. (2019). Catalogo parametrico dei terremoti Italiani (CPTI15), versione 2.0 (Rome: Istituto Nazionale di Geofisica e Vulcanologia (INGV)). Available at <https://emidius.mi.ingv.it/CPTI15-DBMI15/>.
- Rovida, A., Locati, M., Camassi, R., Lolli, B., and Gasperini, P. (2020). The Italian earthquake catalogue CPTI15. *Bull. Earthq. Eng.* 18 (7), 2953–2984. doi:10.1007/s10518-020-00818-y
- Sano, Y., and Marty, B. (1995). Origin of carbon in fumarolic gas from island arcs. *Chem. Geol.* 119, 265–274. doi:10.1016/0009-2541(94)00097-R
- Sano, Y., Nakamura, Y., and Wakita, H. (1985). Areal distribution of ratios in the Tohoku district, Northeastern Japan. *Chem. Geol. Isot. Geosci. Sect.* 52, 1–8. doi:10.1016/0168-9622(85)90004-1
- Sano, Y., Tominaga, T., and Williams, S. N. (1997). Secular variations of helium and carbon isotopes at Galeras volcano, Colombia. *J. Volcanol. Geotherm. Res.* 77 (1–4), 255–265. doi:10.1016/S0377-0273(96)00098-4
- Scarf, L., Barberi, G., Barreca, G., Cannavo, F., Koulakov, I., and Patane, D. (2018). Slab narrowing in the central mediterranean: The calabro-ionian subduction zone as imaged by high resolution seismic tomography. *Sci. Rep.* 8, 5178. doi:10.1038/s41598-018-23543-8
- Schenk, V. (1981). Synchronous uplift of the lower crust of the Ivrea Zone and of southern Calabria and its possible consequences for the Hercynian orogeny in southern Europe. *Earth Planet. Sci. Lett.* 56, 305–320. doi:10.1016/0012-821x(81)90136-9
- Schenk, V. (1980). U-Pb and Rb-Sr radiometric dates and their correlation with metamorphic events in the granulite facies basement of the Serre, southern Calabria (Italy). *Contr. Mineral. Pet.* 73, 23–38. doi:10.1007/bf00376258
- Shimabukuro, D. H., Wakabayashi, J., Alvarez, W., and Chang, S.-C. (2012). Cold and old: The rock record of subduction initiation beneath a continental margin, Calabria, southern Italy. *Lithosphere* 4 (6), 524–532. doi:10.1130/L222.1
- Sizova, E., Hauzenberger, C., Fritz, H., Faryad, S. W., and Gerya, T. (2019). Late orogenic heating of (ultra)high pressure rocks: Slab rollback vs. slab breakoff. *Geosciences* 9 (12), 499. doi:10.3390/geosciences9120499
- Skelton, A. (2011). Flux rates for water and carbon during greenschist facies metamorphism: Geology. *Geology* 39, 43–46. doi:10.1130/G31328.1
- Sketsiou, P., De Siena, L., Gabrielli, S., and Napolitano, F. (2021). 3-D attenuation image of fluid storage and tectonic interactions across the Pollino fault network. *Geophys. J. Int.* 226 (1), 536–547. doi:10.1093/gji/ggab109
- Spakman, W., and Wortel, R. (2004). “A tomographic view on western Mediterranean geodynamics,” in *the TRANSMED Atlas. The Mediterranean region from crust to mantle*. Editors W. Cavazza, F. Roure, W. Spakman, G. M. Stampfli, and P. A. Ziegler (Heidelberg, Germany: Springer-Verlag), 31–52.
- Stampfli, G. M., and Borel, G. D. (2002). A plate tectonic model for the Paleozoic and Mesozoic constrained by dynamic plate boundaries and restored synthetic oceanic isochrons. *Earth Planet. Sci. Lett.* 196 (1–2), 17–33. doi:10.1016/S0012-821x(01)00588-x
- Tamburello, G., Pondrelli, S., Chiodini, G., and Rouwet, D. (2018). Global-scale control of extensional tectonics on CO₂ Earth degassing. *Nat. Commun.* 9, 4608. doi:10.1038/s41467-018-07087-z
- Tansi, C., Tallarico, A., Iovine, G., Gallo, M. F., and Falcone, G. (2005). Interpretation of radon anomalies in seismotectonic and tectonic-gravitational settings: the South-Eastern crati graben (northern Calabria, Italy). *Tectonophysics* 396, 181–193. doi:10.1016/j.tecto.2004.11.008
- Thomson, S. N. (1998). Assessing the nature of tectonic contacts using fission-track thermochronology: An example from the Calabrian arc, southern Italy. *Terra nova*. 10, 32–36. doi:10.1046/j.1365-3121.1998.00165.x
- Thomson, S. N. (1994). Fission track analysis of the crystalline basement rocks of the Calabrian Arc, southern Italy: Evidence of Oligo-Miocene late orogenic extension and erosion. *Tectonophysics* 238, 331–352. doi:10.1016/0040-1951(94)90063-9
- Tiberti, M. M., Vannoli, P., Fracassi, U., Burrato, P., Kastelic, V., and Valensise, G. (2017). Understanding seismogenic processes in the Southern Calabrian Arc: A geodynamic perspective. *Italian J. Geosciences* 136 (3), 365–388. doi:10.3301/ijg.2016.122016.12
- Tortorici, G., Bianca, M., De Guidi, G., Monaco, C., and Tortorici, L. (2003). Fault activity and marine terracing in the capo vaticano area (southern Calabria) during the middle-late quaternary. *Quatern. Int.*, 269–278.
- Tortorici, L. (1982b). - lineamenti geologico strutturalidell'Arco calabro-peloritano. *Rend. Soc. It. Mineral. Pet.* 38 (3), 927–940.
- Tortorici, L. (1982a). -Analisi delle Deform. fragili dei sedimenti postorogeni della Calabr. *Settecentrale.Boll. Soc. Geol.It.* 100 (3), 291–380.
- Tortorici, L. (1981). Analisi delle deformazioni fragili postorogene della Calabria settentrionale. *Boll. Soc. Geol. It* 100, 291–308.
- Tortorici, L., Monaco, C., Tansi, C., and Cocina, O. (1995). Recent and active tectonics in the Calabrian arc (southern Italy). *Tectonophysics* 243, 37–55. doi:10.1016/0040-1951(94)00190-k
- Tursi, F., Acquafredda, P., Festa, V., Fornelli, A., Langone, A., Micheletti, F., et al. (2021). What can high-*P* sheared orthogneisses tell us? An example from the curinga-girifalco line (Calabria, southern Italy). *J. Metamorph. Geol.* 39, 919–944. doi:10.1111/jmg.12596
- Tursi, F., Bianco, C., Brogi, A., Caggianelli, A., Prosser, G., Ruggieri, G., et al. (2020). Cold subduction zone in northern Calabria (Italy) revealed by lawsonite-clinopyroxene blueschists. *J. Metamorph. Geol.* 38 (5), 451–469. doi:10.1111/jmg.12528

- Valley, J. W., and Cole, D. R. (2019). Stable isotope geochemistry. De Gruyter. Available at: <https://www.perlego.com/book/864975/stable-isotope-geochemistry-pdf.1st-ed>.
- Vespasiano, G., Apollaro, C., Muto, F., Dotsika, E., De Rosa, R., and Marini, L. (2014). Chemical and isotopic characteristics of the warm and cold waters of the Luigiane Spa near Guardia Piemontese (Calabria, Italy) in a complex faulted geological framework. *Appl. Geochem.* 41, 73–88. doi:10.1016/j.apgeochem.2013.11.014
- Vespasiano, G., Apollaro, C., De Rosa, R., Muto, F., Larosa, S., Fiebig, J., et al. (2015c). The small spring method (SSM) for the definition of stable isotope - elevation relationships in northern Calabria (southern Italy). *Appl. Geochem.* 63, 333–346. doi:10.1016/j.apgeochem.2015.10.001
- Vespasiano, G., Apollaro, C., Muto, F., De Rosa, R., and Critelli, T. (2015a). Preliminary geochemical and geological characterization of the thermal site of Spezzano Albanese (Calabria, South Italy). *Rend. Online Soc. Geol. It* 33, 108–110. doi:10.3301/rol.2015.26
- Vespasiano, G., Apollaro, C., Muto, F., De Rosa, R., Dotsika, E., and Marini, L. (2015b). Preliminary geochemical characterization of the warm waters of the Grotta delle Ninfe near Cerchiara di Calabria (South Italy). *Rend. Online Soc. Geol. It* 39, 130–133.
- Vespasiano, G., Marini, L., Apollaro, C., and De Rosa, R. (2016). Preliminary geochemical characterization of the thermal waters of Caronte SPA springs (Calabria, South Italy). *Rend. Online Soc. Geol. It* 39, 138–141. doi:10.3301/rol.2015.159
- Vespasiano, G., Marini, L., Muto, F., Auqué, L. F., Cipriani, M., De Rosa, R., et al. (2021). Chemical, isotopic and geotectonic relations of the warm and cold waters of the Cotronei (Ponte Coniglio), Bruciarello and Repole thermal areas, (Calabria - southern Italy). *Geothermics* 96, 102228. doi:10.1016/j.geothermics.2021.102228ISSN 0375-6505
- Vespasiano, G., Muto, F., Apollaro, C., and De Rosa, R. (2012). Preliminary hydrogeochemical and geological characterization of the thermal aquifer in the Guardia Piemontese area (Calabria, south Italy). *Rend. Online Soc. Geol. It* 21, 841–842.
- Vitale, S., Ciarcia, S., Fedele, L., and Tramparulo, F. D. A. (2019). The Ligurian oceanic successions in southern Italy: The key to decrypting the first orogenic stages of the southern Apennines- Calabria chain system. *Tectonophysics* 750, 243–261. <https://doi.org/10.1016/j.tecto.2018.11.010>
- Vogel, J. C., Grootes, P. M., and Mook, W. G. (1970). Isotopic fractionation between gaseous and dissolved carbon dioxide. *Z. Phys.* 230 (3), 225–238. doi:10.1007/bf01394688
- Von Blanckenburg, F., and Davies, J. H. (1995). Slab breakoff – A model for syncollisional magmatism and tectonics in the alps. *Tectonics* 14, 120–131. doi:10.1029/94tc02051
- Westaway, R. (1993). Quaternary uplift of southern Italy. *J. Geophys. Res.* 98, 21741–21772. doi:10.1029/93jb01566
- Zanettin Lorenzoni, E. (1982). Relationships of main structural elements of Calabria (southern Italy). *njgpm.* 7, 403–418. doi:10.1127/njgpm/1982/1982/403
- Zarlenga, F. (2011). Le possibilit' a di utilizzo della risorsa geotermica a Bassa e media entalpia per la sostenibilit' a della produzione energetica. *Energ. Ambiente Innov.* 3, 31–40.
- Zeck, S. E. (1990). *The exhumation and preservation of deep continental crust in the northwestern Calabrian arc, southern Italy*. Santa Barbara [PhD Thesis]: University of California, 277.
- Zhang, M., Zhang, L., Zhao, W., Guo, Z., Xu, S., Sano, Y., et al. (2021). Metamorphic CO₂ emissions from the southern Yadong-Gulu rift, Tibetan Plateau: Insights into deep carbon cycle in the India-Asia continental collision zone. *Chem. Geol.* 584, 120534. doi:10.1016/j.chemgeo.2021.120534ISSN 0009-2541